J. Plasma Physics (2000), *vol.* 63, *part* 2, *pp.* 157–190. Printed in the United Kingdom
© 2000 Cambridge University Press

Global drift waves in weakly ionized magnetized plasmas: theory and observations

PETRO P. SOSENKO,[1,3] GÉRARD BONHOMME[1]
and THIÉRY PIERRE[2]

[1] LPMIA, Université Henri Poincaré – Nancy I, BP 239, 54506 Vandoeuvre les Nancy, Cedex, France

[2] Equipe Turbulence Plasma de l'UMR 6633 CNRS–Université de Provence Case 321, Centre de Saint Jérôme, Av. Escadrille Normandie–Niemen F-13397 Marseille Cedex 20, France

[3] International Centre of Physics and M.M. Boholiubov Institute for Theoretical Physics, 252143, Kyïv, Ukraïna

(Received 13 April 1999 and in revised form 28 June 1999)

Abstract. Properties of global drift waves in a cylindrical weakly ionized magnetized plasma are studied analytically, and are compared with experimental observations.

1. Introduction

The purpose of this paper is to study analytically the properties of global drift waves in a cylindrical weakly ionized magnetized plasma, and to compare them with experimental observations. The important role of drift waves in magnetized plasmas is well known, and they continue to be the subject of intense investigation (for fusion plasmas, for astrophysical and ionospheric plasmas, and for plasmas in laboratory devices).

The basic model for global drift waves (Sec. 2) is derived within the context of the self-consistent field description of collisional plasmas, based on fluid equations and proposed by Tonks and Langmuir (1929). The drift waves are low-frequency (as compared with the ion cyclotron frequency) oscillations, and the drift approximation (Braginskii 1965; Kadomtsev 1965; Sitenko and Malnev 1995), is applied to their investigation, as usual.

The reduced nonlinear model is derived in Sec. 2.2. It allows one to generalize the previous linear analyses (Kadomtsev 1965; Ellis and Marden-Marshall 1979; Ellis et al. 1980; Marden-Marshall et al. 1986; Marden-Marshall and Hall 1986), as well as the original nonlinear models (Kadomtsev 1965; Hasegawa and Mima 1978; Hasegawa and Wakatani 1983, 1984), for weakly ionized plasmas, with global effects, important for large-scale structures, being taken into account.

The simplest nonlinear model for global drift waves follows in the adiabatic regime (Sec. 2.3), when the electron density perturbation is governed by the Boltzmann law (Tonks and Langmuir 1929).

The electron density response to the oscillation field is calculated taking account of the temperature profile effect in Sec. 2.4, which is a simple generalization of the well-known result (Kadomtsev 1965; Ellis and Marden-Marshall 1979) for

https://doi.org/10.1017/S002237789900803X Published online by Cambridge University Press

a collisional plasma. This response allows one to introduce the basic instability mechanisms.

The basic equation for global plasma oscillations is formulated in Sec. 3, and compared with the results of the local theory. The simplest case of flat density and temperature profiles is presented.

Analytical solutions to the eigenvalue problem for the Gaussian density profile and constant temperature are obtained in Sec. 4, and compared with earlier numerical studies (Ellis and Marden-Marshall 1979; Ellis et al. 1980). It is shown that in this case the problem is equivalent to the 'quantum oscillator' problem.

Analytical solutions to the eigenvalue problem, which are related to Bessel functions, are found in the moderate-radius approximation in Sec. 4.1. Exact analytical solutions to the eigenvalue problem, which are related to confluent hypergeometric functions, are presented in Sec. 4.2. Simple analytical expressions for the eigenfrequencies are found in the large-radius approximation in Sec. 4.3.

The basic properties of the confluent hypergeometric functions are listed in Appendix A. The exact and approximate eigenfunctions are traced in Appendix B, together with eigenfrequencies and growth-damping rates.

Taking account of the solution to the eigenvalue problem, the well known local dispersion equation (Kadomtsev 1965) for collisional drift instabilities is reinterpreted for global waves, and possible instability mechanisms are explained in Sec. 5. The approximation of weak non-adiabatic effects is introduced in a usual way. Several particular cases are considered: convective-cell and electron-drift modes, drift dissipative instability when ion–neutral collisions are negligible, drift dissipative instability when ion–neutral collision is an essential stabilization mechanism, weak drift dissipative instability (Sec. 5.1) and weak current convective instability (Sec. 5.2).

Integral constraints are derived for the general case of arbitrary density and temperature profiles, and eigenfrequencies and instability rates are analysed on this basis in Sec. 6.

The analytical theory is compared with earlier numerical results and experimental observations in Sec. 7. Basic plasma parameters, which determine possible physical regimes for global oscillations are introduced and evaluated in Secs 7.1 and 7.2. In particular, the experimental conditions in double cylindrical plasma devices, such as Mirabelle and KIWI, are analysed. Basic plasma parameters and global theory predictions are compared for argon and helium plasmas in Sec. 7.3. Section 8 gives conclusions.

2. Basic model

2.1. Fluid description and drift approximation

Let us start with the self-consistent field description of collisional plasmas, based on fluid equations and proposed by (Tonks and Langmuir 1929).

The electron and ion fluids are described by the continuity equations and the momentum balance equations:

$$\partial_t n_a + \boldsymbol{\nabla} \cdot (n_a \mathbf{v}_a) = \nu_{pa} n_a, \tag{1}$$

$$(\partial_t + \mathbf{v}_a \cdot \boldsymbol{\nabla})\, \mathbf{v}_a = \frac{q_a}{m_a} \left(\mathbf{E} + \frac{1}{c}\, \mathbf{v}_a \times \mathbf{B} \right) - \frac{1}{m_a n_a}\, \boldsymbol{\nabla} p_a - (\nu_a + \nu_{pa})\, \mathbf{v}_a\,, \tag{2}$$

https://doi.org/10.1017/S002237789900803X Published online by Cambridge University Press

where $n_a(\mathbf{r},t)$ is the density, $\mathbf{v}_a(\mathbf{r},t)$ the fluid velocity and $p_a(\mathbf{r},t)$ the scalar pressure for plasma species a. The terms $\nu_p n$ represent particle sources (e.g. ionization) or sinks. The usual terms $\nu\mathbf{v}$ in (2) take account of dissipation due to collisions with neutrals in a partially ionized plasma. The motion of neutrals is disregarded.

According to the original fundamental idea of Tonks and Langmuir (1929), the electromagnetic fields are determined self-consistently from the Maxwell equations. In the case of a potential electric field $\mathbf{E} = -\boldsymbol{\nabla}\Phi$, only the Poisson equation is relevant:

$$\boldsymbol{\nabla}\cdot\mathbf{E} = 4\pi\left(\sum_a q_a n_a + \rho^{\text{ext}}\right), \tag{3}$$

where $\mathbf{B} \equiv B\mathbf{b}$ is an external or mean magnetic field (taken to be static and uniform) and ρ^{ext} is the external charge density.

For slow plasma motion, with characteristic frequencies ω and ν_a much smaller than the cyclotron frequency $\boldsymbol{\Omega}_a$ ($\boldsymbol{\Omega} \equiv qB/mc$, $q_e = -e$, $q_i = Z_i e$),

$$\omega,\ \nu_i,\ \nu_p \ll \boldsymbol{\Omega}_i, \qquad \nu_e \ll \boldsymbol{\Omega}_e, \tag{4}$$

the fluid velocity follows from (2) as the sum

$$\mathbf{v} = \mathbf{v}_d + \mathbf{v}_E + \mathbf{v}_\parallel + \mathbf{v}^{\text{pol}} \tag{5}$$

of the diamagnetic drift velocity

$$\mathbf{v}_d = \frac{1}{mn\boldsymbol{\Omega}}\,\mathbf{b}\times\boldsymbol{\nabla}p, \qquad \boldsymbol{\nabla}\cdot(n\mathbf{v}_d) = 0, \tag{6}$$

the electric field drift velocity (Hall speed)

$$\mathbf{v}_E = \frac{c}{B}\,\mathbf{E}\times\mathbf{b}, \qquad \boldsymbol{\nabla}\cdot\mathbf{v}_E = 0 \tag{7}$$

(which is charge- and mass-independent), the part $\mathbf{v}_\parallel$ taking account of the motion along $\mathbf{B}$, and the polarization drift velocity

$$\mathbf{v}^{\text{pol}} = \frac{1}{\boldsymbol{\Omega}}\,(\partial_t + \nu' + \mathbf{v}\cdot\boldsymbol{\nabla})\,\mathbf{b}\times\mathbf{v}, \qquad \nu' \equiv \nu + \nu_p. \tag{8}$$

Since the latter is a small correction of order λ, one can approximate the fluid velocity in the expression for the polarization drift velocity as

$$\mathbf{v} = \mathbf{v}_E + \mathbf{v}_d + \mathbf{v}_\parallel + \ldots\quad . \tag{9}$$

The electron polarization drift can be disregarded, since $m_e \ll m_i$.

Keeping in mind the situations with $p_e \gg p_i$, one can disregard the effects of finite ion pressure, putting

$$p_i = 0\,. \tag{10}$$

The approximation of isothermal electrons is frequently used to close the system of fluid equations. If needed, one can take account of a fixed spatial dependence of the electron temperature

$$p_e = n_e T_e\ , \qquad T_e = T_e(\mathbf{r})\,, \tag{11}$$

or of electron temperature fluctuations.

2.2. Reduced nonlinear model

With the parallel electron motion and possible global perturbations of equilibrium being included, the reduced transport equations in the drift approximation take

https://doi.org/10.1017/S002237789900803X Published online by Cambridge University Press

the form

$$(\partial_t - \nu_p + \mathbf{v}_E \cdot \boldsymbol{\nabla})\, n_e + \nabla_\parallel (n_e \mathbf{v}_{\parallel e}) = 0\,, \tag{12}$$

$$(\partial_t - \nu_p + \mathbf{v}_E \cdot \boldsymbol{\nabla}) \left(n_e - \frac{\Delta\Phi + 4\pi\rho^{\rm ext}}{4\pi e} \right) + \boldsymbol{\nabla} \cdot \left[\mathbf{v}_i^{\rm pol} \left(n_e - \frac{\Delta\Phi + 4\pi\rho^{\rm ext}}{4\pi e} \right) \right] = 0, \tag{13}$$

$$(d_t + \mathbf{v}_{de} \cdot \boldsymbol{\nabla} + \mathbf{v}_{\parallel e} \nabla_\parallel + \nu_e')\mathbf{v}_{\parallel e} = \frac{e}{m_e}\, \nabla_\parallel \Phi - \frac{1}{m_e n_e}\, \nabla_\parallel (n_e T_e)\,, \tag{14}$$

where the Poisson equation is used to eliminate the ion density, the parallel ion motion is neglected as usual (Ellis et al. 1980), and

$$d_t \equiv \partial_t - \frac{c}{B} \boldsymbol{\nabla}\Phi \times \mathbf{b} \cdot \boldsymbol{\nabla}\,. \tag{15}$$

The term $\mathbf{v}_{de} \cdot \boldsymbol{\nabla} \mathbf{v}_{\parallel e}$ in (14) must be dropped, since a more consistent treatment reveals the well known cancelation of this term with the contribution from $\boldsymbol{\nabla} \cdot \boldsymbol{\pi} \cdot \mathbf{b}$, the collisionless part of the stress tensor, when the latter is taken into account. For sufficiently large ν_e, the electron inertia can be disregarded, and (14) yields

$$v_{\parallel e} = \frac{1}{m_e \nu_e'}\, (e\nabla_\parallel \Phi - T_e \nabla_\parallel \ln n_e), \qquad \nabla_\parallel T_e = 0. \tag{16}$$

If there is an equilibrium electron drift along the magnetic field produced by a constant electric field E_0 then its velocity is

$$U = -\frac{eE_0}{m_e \nu_e'}\,,$$

the potential in the basic equations is replaced according to

$$\nabla_\parallel \Phi \to \nabla_\parallel \Phi - E_0\,,$$

and (16) is replaced by

$$v_{\parallel e} = U + \frac{1}{m_e \nu_e'}\, (e\nabla_\parallel \Phi - T_e \nabla_\parallel \ln n_e)\,. \tag{17}$$

In this approximation, the electron continuity equation is

$$(d_t + U\nabla_\parallel - \nu_p) n_e = \frac{1}{m_e \nu_e'}\, \nabla_\parallel (T_e \nabla_\parallel n_e - e n_e \nabla_\parallel \Phi)\,. \tag{18}$$

For quasineutral motions, the reduced ion continuity equation (13) simplifies to

$$(d_t + \nu_i')\, \Delta\Phi + \boldsymbol{\kappa}_{ne} \cdot (d_t + \nu_i')\, \boldsymbol{\nabla}_\perp \Phi = \frac{4\pi e}{\varepsilon}\, (d_t - \nu_p) n_e\,. \tag{19}$$

with

$$\boldsymbol{\kappa}_Q \equiv \boldsymbol{\nabla} \ln Q, \qquad \varepsilon = 1 + \frac{4\pi n_e m_i c^2}{B^2} \gg 1\,. \tag{20}$$

In the case (16), this model is similar to the Hasegawa–Wakatani model (Hasegawa and Wakatani 1983, 1984), if the approximation of small-scale and small-amplitude oscillations is adopted (the term with κ_{ne} is then disregarded), and if $U = 0$.

Equations (12) (or 18), (13) and (14) give the basic reduced model for the low-frequency oscillations in the weakly ionized magnetized plasma. It is valid in the general case of arbitrary equilibrium and arbitrary oscillation magnitudes.

https://doi.org/10.1017/S002237789900803X Published online by Cambridge University Press

2.3. Adiabatic regime

The coefficient (Self and Ewald 1966) $D_e = T_e/m_e\nu_e'$ determines electron diffusion along the magnetic field direction. According to (18), for rapid enough diffusion, $D_e \to \infty$,

$$\omega \ll \Gamma_\parallel \equiv D_e k_\parallel^2 \to T_e \nabla_\parallel n_e = e n_e \nabla_\parallel \Phi, \tag{21}$$

and the electron density obeys the Boltzmann law

$$n_e = n_{e0} \exp\left[\frac{e(\Phi - \Phi_0)}{T_e}\right], \qquad \nabla_\parallel n_{e0} = 0\,, \tag{22}$$

where Φ_0 is the z-independent part of the equilibrium potential and n_{e0} is the equilibrium electron density in the absence of potential perturbations. In this adiabatic approximation, the ion continuity equation (13) reduces to a closed equation for the electric field potential, which is as follows for quasineutral motions:

$$(d_t + \nu_i')\Delta\Phi + \left\{\boldsymbol{\nabla}\left[\ln n_{e0} + \frac{e(\Phi - \Phi_0)}{T_e} - \frac{\Delta\Phi + 4\pi\rho^{\rm ext}}{4\pi e n_{e0}}\right]\right\} \cdot (d_t + \nu_i')\, \boldsymbol{\nabla}_\perp \Phi$$
$$= \frac{B\Omega_i}{c}\left(1 + \frac{\Delta\Phi + 4\pi\rho^{\rm ext}}{4\pi e n_{e0}}\right)\left\{d_t\left[\ln n_{e0} + \frac{e(\Phi - \Phi_0)}{T_e}\right] - \nu_p\right\}. \tag{23}$$

This equation generalizes the model of Hasegawa and Mima (1978) for the situations of weakly ionized plasmas, with large-magnitude or large-scale oscillations and arbitrary equilibrium states. In particular, the ratio $e\Phi/T_e$ can be of the order of unity, which is sometimes the experimental situation.

2.4. Electron density perturbation

It is convenient to use dimensionless space-time coordinates and the scales $\rho_s = c_s/\Omega_i$ and Ω_i ($c_s^2 = Z_i\bar{T}/m_i$), and to introduce dimensionless variables $n_e/\bar{n} \to n_e$ and $e\Phi/\bar{T} = \phi$, with $\bar{n}$ and $\bar{T}$ some reference values of the electron density and temperature.

The reduced electron continuity equation is expressed in terms of these dimensionless variables as

$$(\partial_t + U\nabla_\parallel + \mathbf{b} \times \boldsymbol{\nabla}\delta\phi \cdot \boldsymbol{\nabla} - \nu_p)\frac{\delta n_e}{n_{e0}} + \mathbf{v}_* \cdot \boldsymbol{\nabla}\delta\phi = D_e \nabla_\parallel^2 \left(\frac{\tau\delta n_e}{n_{e0}} - \delta\phi\right), \tag{24}$$

where the equilibrium axial electron drift with velocity U is taken into account, $\mathbf{v}_* = \boldsymbol{\nabla} \ln n_{e0} \times \mathbf{b}$ is the density-gradient-driven drift velocity, $\tau = T_e/\bar{T}$ is the dimensionless electron temperature, $\nabla_\parallel n_{e0} = 0$, $n_e \equiv n_{e0} + \delta n_e$,

$$D_e = \frac{M}{Z_i \nu_e'}\,, \qquad M = \frac{m_i}{m_e}\,. \tag{25}$$

From here, the density perturbation follows in the linear approximation:

$$\frac{\delta n_e}{n_{e0}} \equiv \tilde{\chi}_e\, \delta\phi, \qquad \delta\phi \equiv \phi.$$

In slab geometry, with the magnetic field along z and the gradients along x, one can look for oscillations in the form

$$\delta\phi \equiv {\rm Re}\hat{\phi}, \qquad \hat{\phi} \sim \exp(ik_y y + ik_z z - i\omega t)\,. \tag{26}$$

In cylindrical geometry, with the magnetic field along z and the gradients in the

https://doi.org/10.1017/S002237789900803X Published online by Cambridge University Press

radial direction only,

$$\delta\phi \equiv \mathrm{Re}\ \hat{\phi}, \qquad \hat{\phi}\ \sim \exp(il\theta + ik_z z - i\omega t)\,. \tag{27}$$

Thus

$$\tilde{\chi}_e = \frac{\omega_* + i\Gamma_\parallel}{\omega - \omega_U + i(\tau\Gamma_\parallel - \nu_p)}, \tag{28}$$

with the drift frequency

$$\omega_* = -\kappa_{n0}k_y, \qquad \kappa_{n0} = \frac{d\ \ln\ n_0}{dx}$$

in slab geometry, and

$$\omega_* = -\frac{l\kappa_{n0}}{r}, \qquad \kappa_{n0} = \frac{d\ \ln\ n_0}{dr}$$

in cylindrical geometry. Here ω_U is the frequency shift in the presence of axial electron flow,

$$\omega_U = \bar{U}k_\parallel\sqrt{\frac{M}{Z_i}}\,,$$

with $\bar{U} = U/s_e$ the ratio of parallel drift velocity and parallel thermal velocity for electrons; $\Gamma_\parallel = D_e k_\parallel^2$ is the rate of electron diffusion along the magnetic field. If the electron inertia is important then ν_e' in $\Gamma_\parallel$ is replaced with $\nu_e' - i(\omega - \omega_U)$. The electron electric susceptibility in the local theory is related to $\tilde{\chi}_e$: $\chi_e(\mathbf{k},\omega) = \tilde{\chi}_e/k^2\lambda_e^2$ in dimensional units, with $\lambda_e^2 = T_e/4\pi e^2 n_{e0}$. In Ellis and Marden-Marshall (1979) there is a misprint in the expression for the electron density response, obtained for $\tau = 1$, $\nu_p = 0$: ω_U is missing from the denominator.

When $\Gamma_\parallel$ is much larger than all other frequencies in (28), the electron density perturbation is governed approximately by the Boltzmann law:

$$\tilde{\chi}_e = \frac{1}{\tau}\ (1 + i\delta), \tag{29}$$

$$\delta = -\frac{1}{\Gamma_\parallel}\ \left[\omega_* - \frac{1}{\tau}\ (\omega - \omega_U - i\nu_p)\right]\ . \tag{30}$$

Deviations from the Boltzmann law, described by δ, determine possible mechanisms of weak instability.

3. Eigenvalue problem

Basic equation. For both cases of slab and cylindrical geometry, the linearized equation (23) yields the eigenvalue problem:

$$(\Delta + \boldsymbol{\kappa}_{n0}\cdot\boldsymbol{\nabla})\hat{\phi} = -K^2\hat{\phi}, \tag{31}$$

where dimensionless variables are used. The term $\boldsymbol{\kappa}_{n0}\cdot\boldsymbol{\nabla}\hat{\phi}$, with $\boldsymbol{\kappa}_{n0} \equiv \boldsymbol{\nabla}\ \ln\ n_{e0}$, appears as the contribution of the ion polarization drift. It can be essential for large-scale oscillations. In the adiabatic regime, for low-frequency oscillations,

$$K^2 \equiv \frac{\omega_* - \omega/\tau}{\omega + i\nu_i}\,. \tag{32}$$

The drift frequency is constant in the case of constant temperature $\tau = 1$ and an exponential density profile in slab geometry or a Gaussian density profile in

https://doi.org/10.1017/S002237789900803X Published online by Cambridge University Press

cylindrical geometry. Then K^2 can be taken as a constant eigenvalue, which is real and positive according to the integral constraint (66), and

$$\omega = \frac{\omega_* - i\nu_i K^2}{1 + K^2}\,. \tag{33}$$

In the local theory, K is replaced with k, the wave vector magnitude.

At the plasma boundary, $\hat{\phi} = 0$. In the cylindrical case, (31) yields $\hat{\phi} \sim r^l$ as $r \to 0$, for any density profile with a finite gradient at $r = 0$. Normally $\kappa_{n0} = 0$ at $r = 0$.

Flat density profile. In the case of flat density and temperature profiles, approximated in the simplest way as $n_{e0} = \text{const}$ for $r \leqslant R_0$ and $n_{e0} = 0$ for $r > R_0$, one encounters the Helmholtz equation:

$$\Delta\hat{\phi} = -K^2\hat{\phi}\,. \tag{34}$$

In cylindrical geometry, the eigenfunctions that satisfy the boundary condition $\hat{\phi}(R_0) = 0$ are

$$\hat{\phi}_{ln} \sim J_l(rK_{ln})\, e^{il\theta}\,, \tag{35}$$

where $J_l(x)$ is the lth order Bessel function, with $x^2J_l'' + xJ_l' + (x^2 - l^2)J_l = 0$, and the 'quantization' condition

$$K_{ln}^2 = \frac{x_{ln}^2 + k_z^2}{R_0^2} \tag{36}$$

holds, where x_{ln} are the zeros of $J_l(x)$.

The eigenfrequencies are

$$\omega = -\frac{i\nu_i}{1 + 1/K_{ln}^2}\,.$$

This mode is purely aperiodic. Its damping is larger for larger mode numbers l and n, for larger k_z^2 and ρ_s, and for smaller plasma radius R_0. The damping is approximately independent of the plasma size for modes with $x_{ln}^2 + k_z^2 \gg R_0^2$.

The numerical values of x_{ln} can be found in Abramowitz and Stegun (1964), or calculated by standard software applications. For example, *Maple V Release 4* easily finds the zeros.

4. 'Quantum oscillator' case

The Gaussian density profile

$$n_0 \sim \exp\left(-\frac{r^2}{r_0^2}\right) \tag{37}$$

is encountered frequently in experiments in cylindrical plasma devices (Latten et al. 1995; Klinger et al. 1997b).

The substitution $\hat{\phi} = \phi'/\sqrt{n_0}$ makes (31) the Schrödinger equation with the potential determined by the density profile:

$$\left(-\tfrac{1}{2}\,\Delta + V\right)\phi' = \tfrac{1}{2}\,K^2\phi', \tag{38a}$$

$$V = \tfrac{1}{4}\,(\boldsymbol{\nabla}\cdot\boldsymbol{\kappa}_{n0} + \tfrac{1}{2}\,\kappa_{n0}^2)\,. \tag{38b}$$

https://doi.org/10.1017/S002237789900803X Published online by Cambridge University Press

It is convenient to introduce a new radial variable normalized to r_0:

$$(-\tfrac{1}{2}\,\Delta + \tfrac{1}{2}\tilde{r}^2)\phi' = E\phi', \tag{39a}$$

$$\tilde{r} = \frac{r}{r_0}, \qquad E = 1 + \tfrac{1}{2}\,K^2 r_0^2. \tag{39b}$$

This is the Schrödinger equation for a two-dimensional harmonic oscillator with unit mass, frequency and Planck's constant. If the motion of the oscillator is considered in rectangular coordinates then the motion in each dimension is independent: there are two harmonic oscillators, each of which can be quantized independently:

$$E = n_1 + \tfrac{1}{2} + n_2 + \tfrac{1}{2} = N + 1 \Rightarrow K^2 = \frac{2N}{r_0^2}$$

where n_1, n_2 and N are non-negative integers. If cylindrical coordinates are used then

$$E = l + 2n + 1 = N + 1 \Rightarrow K^2 = \frac{2N}{r_0^2}, \tag{40}$$

where $l \geqslant 0$ is the azimuthal quantum number, which is the mode number in the plasma case, and $n \geqslant 0$ is the radial quantum number.

The boundary condition for the plasma eigenvalue problem is different from that for the quantum oscillator. One must consider a two-dimensional potential well that is of circular form with a $\frac{1}{2}r^2$ bottom and that is infinite at the plasma boundary $\tilde{r} = R_0/r_0$. However, the form of the eigenvalue equation shows explicitly that there is a discrete spectrum, and suggests some analytical approximations.

4.1. Moderate-radius approximation

When the energy level is far above the well bottom,

$$E \gg \frac{R_0^2}{2r_0^2}\,, \tag{41}$$

then the bottom shape can be disregarded, and the Schrödinger equation reduces to the Helmholtz equation: $\Delta\phi' + 2E\phi' = 0$. The eigenvalues and eigenfunctions are

$$K_{ln}^2 = \frac{2(E_{ln} - 1)}{r_0^2} \approx \frac{x_{ln}^2}{R_0^2}, \tag{42a}$$

$$\hat{\phi}_{ln} \sim \exp\left(\frac{r^2}{2r_0^2}\right) J_l\left(\frac{r x_{ln}}{R_0}\right)\, e^{il\theta}, \tag{42b}$$

$$\mathrm{Re}\;\omega = \frac{2l/r_0^2}{1 + x_{ln}^2/R_0^2}\,. \tag{42c}$$

The Helmholtz approximation can be used if

$$\frac{R_0^2}{r_0^2} < x_{ln}\,, \tag{43}$$

when (41) is satisfied. In this approximation the parameter

$$S \equiv R_0^2 K^2 = x_{ln}^2 - \frac{2R_0^2}{r_0^2} \approx x_{ln}^2$$

depends very weakly on the plasma radius R_0, which is in agreement with the numerical results for S (Ellis et al. 1980). The approximation (43) is easier to satisfy

https://doi.org/10.1017/S002237789900803X Published online by Cambridge University Press

for $R_0^2/r_0^2 \lesssim 1$ (plasma columns of moderate radius), while the case $R_0^2/r_0^2 \gg 1$ (plasma columns of large radius) requires sufficiently high mode numbers. The limit $R_0^2/r_0^2 \ll 1$ corresponds to small density gradients (flat density profile).

4.2. Exact solution

The exact solution to (31) with the Gaussian density profile, or to (39), can be found by standard methods presented in textbooks on quantum mechanics. One first determines the solution behaviour when $r \to 0$, according to the condition of finite $\phi(0)$, and then seeks a solution in the form of a power series in r, with the coefficients being determined by recurrence relations. In this way, the potential perturbation is expressed in terms of the confluent hypergeometric function $M(a, b, z)$ (see Appendix A):

$$\hat{\phi} \sim r^l \, e^{il\theta} M\left(\frac{2l - K^2 r_0^2}{4},\ l+1,\ \frac{r^2}{r_0^2}\right), \qquad l \geqslant 0\,. \tag{44}$$

The boundary condition $\phi(R_0) = 0$ yields the eigenvalues

$$K^2 r_0^2 = 2l - 4a_{ln}\left(\frac{R_0^2}{r_0^2}\right), \tag{45}$$

with $a_{ln}(z)$ a real root of the equation $M(a, l+1, z) = 0$,

$$a_{ln} + n < 0 \Rightarrow K^2 r_0^2 > 2(l+2n)\,.$$

The eigenfrequency in the adiabatic regime is

$$\omega = \frac{l}{l - 2a_{ln} + \frac{1}{2}r_0^2}, \qquad \omega_* = \frac{2l}{r_0^2}, \tag{46}$$

with the validity condition

$$r_0^2 - 4a_{ln} \gg 2l\,. \tag{47}$$

One can calculate the ratio of exact and approximate results for K^2:

$$\frac{2l - 4a_{ln}}{x_{ln}^2}\left(\frac{R_0}{r_0}\right)^2.$$

For example, when $R_0^2/r_0^2 = 2$, $n = 0$, this ratio is equal to 0.82 for $l = 1$, to 0.91 for $l = 2$, to 0.95 for $l = 3$, to 0.97 for $l = 4$, to 0.98 for $l = 5$ and 6, and to 0.99 for $l = 7$ and 8. The moderate-radius approximation overestimates the eigenvalue; however, the relative error of about 20% for $l = 1$ reduces to 1% for $l = 8$.

According to the usual boundary conditions in the quantum mechanical treatment, one must require that the wave function ϕ' go to zero when r goes to infinity. Then $M(a, b, z)$ must be a finite polynomial in z, which increases more slowly than the exponential, when $z \to \infty$. Such a condition is satisfied if $-a$ is a non-negative integer, which yields (40). This condition is not applicable in general in the interesting plasma case.

4.3. Large-radius approximation

When $R_0^2/r_0^2 \gg 1$, and l is not very large, then (see Appendix A) $a_{ln} \approx -n$, and

$$K^2 \approx \frac{2(l+2n)}{r_0^2}, \qquad \omega = \frac{l}{l + 2n + \frac{1}{2}r_0^2}, \tag{48}$$

https://doi.org/10.1017/S002237789900803X Published online by Cambridge University Press

with the validity condition $r_0^2/2 + 2n \gg l$. Therefore the 'quantum mechanical' result (40) is formally appropriate in the large-radius approximation.

5. General dispersion equation

With the general electron density response, one finds the dispersion relation

$$K^2 \equiv \frac{\omega_* - \omega\tilde{\chi}_e(\omega)}{\omega + i\nu_i}\,. \tag{49}$$

With the fluid response for electrons (28), in the case $\tau = 1$ and $\nu_p = 0$,

$$K^2 = \frac{i(\omega_* - \omega)\Gamma_\parallel - \omega_*\omega_U}{(\omega + i\nu_i)(\omega - \omega_U + i\Gamma_\parallel)}\,. \tag{50}$$

The quadratic equation for the frequency is

$$\omega^2 + \omega\left[i\Gamma_\parallel\left(1 + \frac{1}{K^2}\right) + i\nu_i - \omega_U\right] - \Gamma_\parallel\left(\nu_i + i\frac{\omega_*}{K^2}\right) + \omega_U\left(\frac{\omega_*}{K^2} - i\nu_i\right) = 0\,. \tag{51}$$

This differs only in notation from the well-known local-theory result presented in (IV.105) on p. 102, (IV.95) on p. 100 and (IV.90) on p. 98 Kadomtsev (1965) (with $\Gamma_\parallel \to \omega_s k^2 r_H^2$, $\rho_s \to r_H$, $K^2 \to k^2 r_H^2$), and used in Ellis and Marden-Marshall (1979) and Ellis et al. (1980). Note that there is an incorrect sign in (IV.85) on p. 97, Kadomtsev (1965), which should read

$$\frac{n_e}{n} = \frac{k_z^2 + i\dfrac{k_y\kappa}{\boldsymbol{\Omega}_e\tau_e}}{D_e k_z^2 - i\omega}\,\frac{e\tau_e}{m_e}\,\phi\,.$$

This sign must be corrected in (IV.86) and (IV.87) of Kadomtsev (1965); however, it does not affect the dispersion relations (IV.105) on p. 102, (IV.95) on p. 100 and (IV.90) on p. 98.

When $\nu_p \neq 0$, one must replace ω with $\tilde{\omega} = \omega - i\nu_p$, and ν_i with $\nu_i + 2\nu_p$.

Weak non-Adiabatic effects. Introducing the deviations from the adiabatic density response for electrons,

$$K^2 \equiv \frac{\omega_* - \omega(1 + i\delta)}{\omega + i\nu_i}\,, \tag{52}$$

in the case of weak non-adiabatic effects, with $|\delta| \ll 1$, and when $K^2 = \text{const}$, one finds by iteration

$$\omega = \frac{\omega_* - i\nu_i K^2}{1 + i\delta + K^2}\,, \tag{53}$$

with the necessary instability condition $\omega_*\ \mathrm{Re}\ \delta < 0$. Expanding in powers of δ, one finds the necessary and sufficient instability condition

$$\nu_i K^2 + \frac{\omega_*\ \mathrm{Re}\ \delta}{1 + K^2} < 0\,. \tag{54}$$

Let us consider some simple limiting cases of the quadratic dispersion equation, which reveal some basic physical regimes.

https://doi.org/10.1017/S002237789900803X Published online by Cambridge University Press

Vorticity mode. If $\Gamma_\parallel, \omega_U \ll \omega_*, \omega$ then $\omega = -i\nu_i$, which is the convective-cell (vorticity) mode in a weakly ionized plasma. In a completely ionized plasma, ν_i is replaced by $\mu_i k^2$ in the local approximation (Okuda and Dawson 1973), with μ_i the ion viscosity.

Electron drift mode. When $\Gamma_\parallel \to \infty$,

$$\omega = \frac{\omega_* - i\nu_i K^2}{1 + K^2},$$

which is the collisional electron drift mode, considered above in the drift approximation. In a completely ionized plasma, ν_i is replaced by $\mu_i k^2$ in the local approximation (see e.g. Hasegawa and Mima 1978), with μ_i the ion viscosity.

Drift-dissipative instability. If $\omega_U = 0$, $\nu_i = 0$ and $K^2 \ll 1$, then one recovers the textbook example of the drift-dissipative instability, (see e.g. Kadomtsev 1965; Sitenko and Malnev 1995): $\omega^2 + i\omega\omega_s - i\omega_s\omega_* = 0$, with the roots

$$\omega_1 = \omega_* + \frac{i\omega_*^2}{\omega_s}, \quad \omega_2 = -i\omega_s, \quad \text{when } \omega_s \gg |\omega_*|,$$
$$\omega_{1,2} = \pm\sqrt{i\omega_s\omega_*}, \quad \text{when } \omega_s \ll |\omega_*|.$$

In dimensional units, $\omega_s = \omega_p^2 k_\parallel^2 / k^2 \alpha_i \nu_e$, with ω_p the electron plasma frequency.

In the interesting case of global modes, one must reinterpret ω_s: $\omega_s = \Gamma_\parallel / K^2$.

Effect of ion–neutral collisions. Ion collisions can stabilize this instability:

$$\omega^2 + i\omega[\omega_s(1 + K^2) + \nu_i] - \omega_s(i\omega_* + \nu_i K^2) = 0\,. \tag{55}$$

From here, $\omega \equiv \omega_r + i\omega_i$, with

$$\omega_r = \pm\frac{\tilde\omega_s}{2\sqrt{2}}\ \mathrm{sign}(\omega_*)\ \sqrt{4\tilde\nu_i - 1 + \sqrt{(1 - 4\tilde\nu_i)^2 + 16\tilde\omega_*^2}}\,,$$
$$\omega_i = \frac{\tilde\omega_s}{2}\left[-1 \pm \frac{1}{\sqrt{2}}\sqrt{1 - 4\tilde\nu_i + \sqrt{(1 - 4\tilde\nu_i)^2 + 16\tilde\omega_*^2}}\right],$$
$$\tilde\omega_s \equiv \omega_s(1 + K^2) + \nu_i\,,$$
$$\tilde\nu_i \equiv \frac{K^2\nu_i\omega_s}{\tilde\omega_s^2} \leqslant \frac{K^2}{4(1 + K^2)} \leqslant \frac{1}{4}\,,$$
$$\tilde\omega_* \equiv \frac{\omega_*\omega_s}{\tilde\omega_s^2} \leqslant \frac{\omega_*}{4\nu_i(1 + K^2)}\,.$$

The stability condition is $\tilde\nu_i^2 \geqslant \tilde\omega_*^2$; that is, $\nu_i^2 \geqslant \omega_*^2 / 4K^2(1 + K^2)$ (the $l = 0$ mode is stable). In the large-radius approximation, when $\omega_* \approx K^2 << 1$, $\nu_i^2 \geqslant \frac{1}{4}\omega_*$.

The instability condition $\tilde\nu_i^2 < \tilde\omega_*^2$ gives the band of ω_s, $x_1\nu_i < \omega_s < x_2\nu_i$, with $x_{1,2}$ the solutions of the quadratic

$$K^2(1 + K^2)^2 x^2 + \left[2K^2(1 + K^2) - \frac{\omega_*^2}{\nu_i^2}\right] x + K^2 = 0.$$

5.1. Weak drift dissipative instability

When $|\tilde\omega_*^2 - \tilde\nu_i| \ll \frac{1}{16}$,

$$\frac{\omega_r}{\tilde\omega_s} = \pm\tilde\omega_*\left[1 - \frac{2(\tilde\omega_*^2 - \tilde\nu_i)}{1 + 4\tilde\nu_i}\right] \approx \pm\tilde\omega_*\,, \tag{56a}$$

https://doi.org/10.1017/S002237789900803X Published online by Cambridge University Press

$$\frac{\omega_i}{\tilde{\omega}_s} = \frac{1}{2}\left[-1 \pm 1 \pm \frac{2(\tilde{\omega}_*^2 - \tilde{\nu}_i)}{1 + 4\tilde{\nu}_i}\right]; \tag{56b}$$

that is, one root is stable (modified convective cell mode) with

$$\omega_i^- \approx -\omega_s(1 + K^2) - \nu_i\,,$$

while another can be unstable, with

$$\omega_i^+ \approx \tilde{\omega}_s\,\frac{\tilde{\omega}_*^2 - \tilde{\nu}_i}{1 + 4\tilde{\nu}_i}\,.$$

The latter expressions for ω_r and ω_i simplify when

$$\Gamma_\parallel \gg \frac{\nu_i K^2}{1 + K^2}, \tag{57}$$

which frequently corresponds to experimental conditions. In this limit, for the stable mode,

$$\omega_r^- \approx -\frac{\omega_*}{1 + K^2}\,, \tag{58a}$$

$$\omega_i^- \approx -\Gamma_\parallel\frac{1 + K^2}{K^2}\,, \tag{58b}$$

while, for the possibly unstable electron drift mode,

$$\omega_r^+ \approx \frac{\omega_*}{1 + K^2}\,, \tag{59a}$$

$$\omega_i^+ \approx \left(\frac{\omega_r^2}{\Gamma_\parallel} - \nu_i\right)\,\frac{K^2}{1 + K^2}\,. \tag{59b}$$

The stability condition is

$$\nu_i\Gamma_\parallel \geqslant \omega_r^2\,. \tag{60}$$

In the large-radius approximation, when $\omega_* \approx K^2 \ll 1$, $n = 0$,

$$\omega_r^+ \approx \frac{\omega_*}{1 + \omega_*}\,, \tag{61a}$$

$$\omega_i^+ \approx \omega_r\left(\frac{\omega_r^2}{\Gamma_\parallel} - \nu_i\right)\,. \tag{61b}$$

The approximate expressions for the real and imaginary parts of the frequency in the limit (57) that are presented in Ellis et al. (1980) and Kauschke et al. (1990) can be used to describe the drift-dissipative instability when $K^2 = 1$ only.

5.2. Current convective instability

In a current-carrying plasma, the drift-dissipative instability can transform into the current convective (or spiral) instability. The possibly unstable solution of the general dispersion equation with $\omega_U \neq 0$ can be presented as

$$\omega_r = \frac{\omega_*\omega_s + \omega_U\nu_i}{\omega_s(1 + K^2) + \nu_i}\,, \tag{62a}$$

$$\omega_i = \frac{\omega_r^2 - \omega_r\omega_U - \nu_i\omega_s K^2 + \omega_U\omega_*/K^2}{\omega_s(1 + K^2) + \nu_i}\,, \tag{62b}$$

when $\omega_i \ll \tilde{\omega}_s$, $\tilde{\omega}_s\omega_r/\omega_U$.

https://doi.org/10.1017/S002237789900803X Published online by Cambridge University Press

In the limit $\omega_s\omega_* \gg \omega_U\nu_i$ and $\omega_s(1+K^2) \gg \nu_i$, these expressions simplify to

$$\omega_r \approx \frac{\omega_*}{1+K^2}\,, \tag{63a}$$

$$\omega_i \approx \left(\frac{\omega_r^2}{\Gamma_\parallel} + \frac{\omega_U\omega_r}{K^2\Gamma_\parallel} - \nu_i\right)\ \frac{K^2}{1+K^2}\,, \tag{63b}$$

and the stability condition is

$$\nu_i\Gamma_\parallel \geqslant \omega_r\left(\omega_r + \frac{\omega_U}{K^2}\right). \tag{64}$$

In the large-radius approximation, when $\omega_* \approx K^2 \ll 1$ and $n = 0$,

$$\omega_r \approx \frac{\omega_*}{1+\omega_*}\,, \tag{65a}$$

$$\omega_i \approx \omega_r\left(\frac{\omega_r^2}{\Gamma_\parallel} + \frac{\omega_U}{\Gamma_\parallel} - \nu_i\right)\,, \tag{65b}$$

and the stability condition is $\nu_i\Gamma_\parallel \geqslant \omega_r^2 + \omega_U$.

The approximate expression presented in Ellis et al. (1980) and Kauschke et al. (1990) (with the following correspondence between the notations: $\nu_\parallel$ or $\nu_z \to \Gamma_\parallel$, $b \to K^2$, $\omega_1 \to \omega_U$),

$$\omega_i \approx \frac{\omega_*}{\nu_\parallel(1+b)}\ \left[\frac{\omega_*}{(1+b)^2} + \omega_1\right] - \nu_i\ \frac{b}{1+b}\,,$$

is valid for the description of the current convective instability mechanism when $K^2 \ll 1$. When both drift dissipative and current convective instability mechanisms are important, and when K^2 is arbitrary, the approximate expression in Ellis et al. (1980) and Kauschke et al. (1990) cannot be used. The latter expression describes correctly for all b the stabilizing mechanism owing to the ion–neutral collisions only. The expression

$$\omega_i \approx \frac{b}{1+b}\ \left[\frac{\omega_*^2}{\nu_\parallel(1+b)^2} + \frac{\omega_1\omega_*}{b\nu_\parallel} - \nu_i\right]$$

(Ellis and Marden-Marshall 1979) correctly represents the drift-dissipative instability mechanism.

6. Integral constraints for arbitrary equilibria

The eigenvalue equation (31) yields the following integral constraint:

$$\int d\mathbf{r}\ n_0\ |\ \boldsymbol{\nabla}\hat{\phi}\ |^2 = \int d\mathbf{r}\ K^2 n_0\ |\ \hat{\phi}\ |^2\ . \tag{66}$$

One derives it after multiplying the eigenvalue equation by $n_0\hat{\phi}^*$ and integrating by parts for zero boundary conditions.

For arbitrary density and temperature profiles, the constraint (66) in the ideal limit takes the form

$$\omega = \frac{1}{W}\int d\mathbf{r}\ n_0\ \omega_*\ |\ \hat{\phi}\ |^2, \tag{67}$$

where

$$W \equiv W_K + W_P = \int d\mathbf{r}\ n_0\left(|\ \boldsymbol{\nabla}\hat{\phi}\ |^2 + \frac{|\ \hat{\phi}\ |^2}{\tau}\right.$$

https://doi.org/10.1017/S002237789900803X Published online by Cambridge University Press

is the total energy, in which the first term is the contribution from the particle kinetic energy

$$W_K = \int d\mathbf{r}\; n_0 \mid \boldsymbol{\nabla}\hat{\phi} \mid^2,$$

while the second term is the potential energy contribution. Thus there are no unstable (or damped) modes in this case. For monotonic density profiles, the eigenfrequency has the sign of ω_*.

With ion–neutral collisions taken into account,

$$\omega = \frac{1}{W} \int d\mathbf{r}\; n_0\; \omega_* \mid \hat{\phi} \mid^2 - i\nu_i\; \frac{W_K}{W}\,, \tag{68}$$

one finds damped plasma oscillations.

With weak deviations from the adiabatic density response for the electrons,

$$\omega = \frac{\displaystyle\int d\mathbf{r}\; n_0 \left[\omega_* \mid \hat{\phi} \mid^2 - i\nu_i \mid \boldsymbol{\nabla}\hat{\phi} \mid^2\right]}{\displaystyle\int d\mathbf{r}\; n_0 \left[\mid \boldsymbol{\nabla}\hat{\phi} \mid^2 + (1 + i\delta) \mid \hat{\phi} \mid^2 / \tau\right]}\,. \tag{69}$$

From here,

$$\omega_r = \frac{1}{W} \int d\mathbf{r}\; n_0\; \omega_* \mid \hat{\phi} \mid^2, \tag{70}$$

$$\omega_i = -\nu_i \frac{W_K}{W} - \frac{\omega_r}{W} \int d\mathbf{r}\; \frac{n_0\; \mathrm{Re}\; \delta \mid \hat{\phi} \mid^2}{\tau}\,, \tag{71}$$

with the necessary instability condition

$$\omega_r \int d\mathbf{r}\; \frac{n_0\; \mathrm{Re}\; \delta \mid \hat{\phi} \mid^2}{\tau} < 0\,. \tag{72}$$

With δ given by (30) in the case of collisional electrons,

$$\omega_i = -\nu_i \frac{W_K}{W} + \frac{\omega_r}{W\Gamma_\parallel} \int d\mathbf{r}\; \frac{n_0}{\tau} \left(\omega_* - \frac{\omega_r - \omega_U}{\tau}\right) \mid \hat{\phi} \mid^2\,. \tag{73}$$

For constant electron temperature $\tau = 1$,

$$\omega_i = \frac{W_K}{W} \left(\frac{\omega_r^2}{\Gamma_\parallel} + \omega_U \omega_r \frac{W_P}{W_K} - \nu_i\right)\,. \tag{74}$$

When $\omega_i/\omega_r \ll 1$, one can compute W_K, W, ω_i with $\mid \hat{\phi} \mid^2$ and $\mid \boldsymbol{\nabla}\hat{\phi} \mid^2$ given by the eigenfunction resulting from the solution to the eigenvalue problem in the ideal case. Experimentally observed temperature and density profiles can be taken into account. If $W_K \ll W_P$ then $\omega_i = \omega_r \omega_U$. If $W_K \gg W_P$ then $\omega_i = \omega_r^2/\Gamma_\parallel - \nu_i$.

For arbitrary density profiles, the general dispersion equation (51) is replaced by

$$\omega^2 + \omega \left[i\Gamma_\parallel \left(1 + \frac{1}{W_K}\right) + i\nu_i - \omega_U\right] - \Gamma_\parallel \left(\nu_i + \frac{i\bar{\omega}_* W_P}{W_K}\right) + \omega_U \left(\frac{\bar{\omega}_* W_P}{W_K} - i\nu_i\right) = 0\,, \tag{75}$$

where

$$\bar{\omega}_* = \frac{1}{W_P} \int d\mathbf{r}\; n_0\; \omega_* \mid \hat{\phi} \mid^2\,. \tag{76}$$

This quadratic form can be used to evaluate ω in the general case.

https://doi.org/10.1017/S002237789900803X Published online by Cambridge University Press

Table 1. Argon plasma parameters in KIWI and Mirabelle: magnetic field B, electron density n_e, pressure p, electron temperature T_e (with the maximum at the centre from the measured temperature profile), midsection diameter d, Gaussian $1/e$ plasma column width r_0, plasma column radius R_0 and length $l_\parallel$, and ratio of axial drift velocity to electron thermal velocity $U/v_{\mathrm{th},\,e}$. The parameters of the toroidal argon plasma in TORIX (LPMI, Ecole Polytechnique) are given for comparison (Gresillon and Tomchuk 1998b).

	B (G)	n_e (cm^{-3})	p (mbar)	T_e (eV)	T_i (eV)
KIWI 1995	700	(1–7) $\times 10^{10}$	5×10^{-4}	0.5–1.5	
KIWI 1997	700	(1–2) $\times 10^{10}$	8×10^{-4}	0.5–1.2	0.03
Mirabelle	0–900	(5–70) $\times 10^{9}$	(0.5–8) $\times 10^{-4}$	2	0.05
TORIX	0–5000	4×10^{10}	7×10^{-4}	0.6–2.5	
	d (cm)	r_0 (cm)	R_0 (cm)	$l_\parallel$ (cm)	$U/v_{\mathrm{th},\,e}$
KIWI 1995	30	2.3	6	160	0–0.4
KIWI 1997	30	2.8	7	160	
Mirabelle	30	7–11	14	140	

Table 2. Argon plasma characteristics corresponding to the parameters in Table 1, for $n_e = 5 \times 10^{10}$ cm^{-3}, $T_e = 1.5$ eV and $T_i = 0.03$ eV.

Ω_i (s^{-1})	f_i (kHz)	α_i (10^5)	β_e	m_e/m_i
168 000	27	0.8	0.6×10^{-5}	1.4×10^{-5}
$v_{\mathrm{th},\,e}$ (m s^{-1})	v_A (m s^{-1})	v_s (m s^{-1})	$v_{\mathrm{th},\,i}$ (m s^{-1})	ρ_s (cm)
5×10^5	10×10^5	2×10^3	300	1

7. Discussion

7.1. Plasma parameters

Observations of collective oscillations in cylindrical argon plasmas have been reported by Latten et al. (1995) for the KIWI device and by Bonhomme et al. (1998) and Gravier et al. (1999) for the Mirabelle device. The parameters of these plasmas are given in Table 1, together with those for the experiments reported by Klinger et al. (1997b) and Grulke et al. (1999) for KIWI and by Pierre et al. (1987) and Pisani et al. (1998) for Mirabelle.

From Table 1, one finds the important plasma characteristics, which are presented in Table 2.

7.2. Double plasma devices

Mirabelle. This is a magnetized double-plasma device constructed in the Laboratoire de Physique des Milieux Ionisés, Université Henri Poincaré in Nancy (Pierre et al. 1987). It consists of two identical cylindrical plasma chambers of diameter 1 m and length 1 m, separated by a column of diameter 30 cm and length 1.4 m, which is immersed in a solenoid. Each plasma chamber is part of the double-plasma device used for ion-acoustic-wave studies. (Pierre et al. 1981, 1983a,b, 1985a,b; Bonhomme et al. 1991). It contains an electrically insulated cylindrical anode with a multipolar magnetic field at the walls, created by many ferrite magnets. The magnetic field of the latter at the surface is roughly 1 kG. The anode is almost closed. The only aperture free of magnets corresponds to the end of the central plasma column. As in the usual double-plasma devices, energetic primary electrons are reflected by the permanent magnets and create a dense, quiet and homogeneous plasma in each chamber.

https://doi.org/10.1017/S002237789900803X Published online by Cambridge University Press

The cathode consists of 24 equally spaced tungsten filaments located on a vertical plane at the end of each source chamber. The maximum field strength is 1800 G, with a current of 1200 A in the solenoid.

Stainless steel grids contain the plasma electrons in both end plasmas. The ionizing electrons can flow across the grids.

In Mirabelle, the plasma is usually created in argon by an electric discharge, at pressures ranging from 5×10^{-5} to 80×10^{-5} Torr. The electron density in the column can be determined by axial and radial Langmuir probes. The density on the axis can be up to $7 \times 10^{10}\,\mathrm{cm}^{-3}$. Because the plasma electrons are strongly magnetized, the electron current collected by the probe is very sensitive to the probe orientation in the column, and the density must be measured by an axial probe.

The filaments emitting the ionizing electrons in the fringing solenoid field of the order of 15 G produce localized primary currents inside the column leading to a predominant light emission along the trajectories of the primaries, and clearly exhibiting the magnetic field line topology. Since the ionization is enhanced inside the primary channels, the density profile can have alternating humps and dips.

In order to cancel this inhomogeneity mechanism, the magnetic field strength must be maintained at a value as low as possible in the filament plane, and also over an axial extent in order to permit the primaries to randomize their trajectories. The primaries are emitted in the region of low magnetic field (< 10 G), and driven to the multipolar walls. There they are randomized after reflection and finally injected inside the column.

The field is shaped by the two compensation coils, whose field counterbalances the fringing solenoid field. Increasing the counteracting field strength makes the null axial magnetic field surface enter the plasma, and the density profile becomes smoother. It is necessary to maintain the cusp near the filaments in order to provide for both a smooth density profile and a high density at the plasma column centre.

The electron temperature is obtained as usual from a semilogarithmic plot of the electron current versus the probe bias. The current is collected by a plane Langmuir probe whose collecting area is large compared with the electron Larmor radius.

The analysis of characteristics recorded with gas pressure increasing from 5×10^{-5} to 40×10^{-5} Torr gives an electron temperature decreasing from 4.25 to 2.5 eV. The dominant cause of such an evolution is variation of the electron-neutral collision frequency. The temperature values do not depend on the magnetic field strength, and are in good agreement with the values given by the velocity of ion acoustic waves that propagate along the magnetized plasma column. The ion temperature is not measured directly. The study of the damping of axial ion acoustic waves allows one to assume the same value (< 0.1 eV), as without the magnetic field.

KIWI (Kiel Instrument for Wave Investigations). This is a large double device, where the plasma is produced in two magnetic box discharges and where the plasma diffuses into a magnetized midsection. This midsection is electrically isolated from the source chambers, and can be separated by two mesh grids. A double-plasma mode is achieved by activating one chamber only and using the grid at the far end of the midsection as a loss surface. This mode was chosen for the experiments, in which a probe array with 64 azimuthally arranged Langmuir probes was used as a new diagnostic tool for plasma oscillations. The probes in the array are operated in the electron saturation regime.

https://doi.org/10.1017/S002237789900803X Published online by Cambridge University Press

A comparison between probe and wave diagnostic methods demonstrated that even in the magnetized plasma the measurements of the plasma parameters are reliable to within 20% for the density, 10% for the temperature and 0.3 V for the plasma potential. The electron temperature profile has a maximum at the centre of the plasma column, because part of the plasma is produced by beam–plasma interaction in the magnetized column. The value of $T_i = 0.03\,\mathrm{eV}$, reported by Klinger et al. (1997b), is inferred from laser diagnostics in a thermionic discharge (Bachet et al. 1993).

The diameter of the plasma column is smaller than in the Mirabelle device (4 cm compared with 16 cm). This is mainly due to a inexact compensation of the fringing field of the solenoid and to a lower diameter of the source chambers. It is worth noting that the effective plasma radius is well defined in Mirabelle owing to a biasable inner tube at the outer edge of the plasma column. This is not the case in the KIWI device. Moreover, the lower plasma radius in this latter device does not allow for a proper determination of the potential at the radial limiting boundary.

$k_\parallel$ estimates and current instability. The critical value for the onset of the current instability is (Latten et al. 1995) $U/v_{\mathrm{th},\,e} = 0.35$. If the critical value is exceeded, coherent modes with mode numbers in the range $l = 1$–3 are destabilized (regular regime). The axial electron drift, which destabilizes plasma oscillations, is used as the dynamical control parameter. It is governed by both the voltage difference $U_{G2} - U_{G1}$ between the grids and the grid bias U_{G1} with respect to the anode potential.

The non-vanishing axial wavenumber can be evaluated as $k_\parallel \approx \pi/l_\parallel \approx 2\,\mathrm{m}^{-1}$, which can be taken as the minimum value $k_{\parallel\min}$. The ratio $v_s k_{\parallel\min}/\Omega_i \approx 0.02$ justifies the neglect of parallel ion motion for the modes with $k_\parallel \approx k_{\parallel\min}$ only.

One can evaluate the Doppler frequency shift

$$\omega_U = U k_\parallel \gtrsim U\pi/l_\parallel \approx 360 \times 10^3\ \mathrm{s}^{-1} \approx 2\Omega_i$$

at the critical value of the velocity ratio and for the minimum $k_\parallel$. This value is well beyond the low-frequency range for electron drift waves.

The electron axial drift is determined experimentally by the ratio of the electron saturation current of a plane probe in upstream and downstream direction. It was demonstrated that this method, proposed originally by Pierre et al. (1992), gives a reliable estimate of the electron axial drift velocity in magnetized plasmas within $0.03 v_{\mathrm{th},\,e}$.

Turbulent regime. In the turbulent regime, a broad range of modes is excited, with the $l = 3$ mode of $k \approx 80\,\mathrm{m}^{-1}$ being dominant (Latten et al. 1995). A least-squares fit of the spectral components $l = 6$–23 gives a power law $S(k) \sim k^{-\alpha}$, with $\alpha = 3.6 \pm 0.1$. A similar exponent was reported in Grésillon and Tomchuk (1998b).

Regular regime. The oscillation characteristics for the mode $l = 2$ in the regular regime measured by Latten et al. (1995) are presented in Table 3. This mode is dominant, while the spectral intensities of modes $l = 1$ and $l = 3$ are fairly weak.

For the $l = 2$, mode already $f_l/f_i = 0.37$, which is on the validity margin for the low-frequency theory of drift waves. In general, plasma modes around the cyclotron frequency are reported to be excited, which means that one must be careful when interpreting the experimental observations in terms of the electron drift wave turbulence.

https://doi.org/10.1017/S002237789900803X Published online by Cambridge University Press

Table 3. Oscillation characteristics measured by Latten et al. (1995) for mode number l, mode frequency f_l, phase velocity $v_{\rm ph} = 2\pi f_l/k_\perp$, wavenumber $k_\perp$ at the radial probe position $r_p \approx 4\,$cm, inverse gradient length $1/L = -\boldsymbol{\kappa}_{n0}$ at the probe location, drift velocity $v_{De} = T_e/eBL$ for $T_e = 1.5\,$eV, and drift frequency $\omega_{De} = v_{De}k_\perp$.

f_l ($l = 2$)	$k_\perp = l/r_p$ (m^{-1})	$1/L$ (m^{-1})	$v_{\rm ph}$ (m s^{-1})	v_{De} (m s^{-1})	ω_{De} (s^{-1})
9.9 kHz	50	70	1270	1000	51×10^3

In the case of the Gaussian density profile, the eigenfrequency in the weakly non-adiabatic regime is

$$\omega_r = \frac{l\Omega_i}{l - 2a_{ln} + r_0^2/2\rho_s^2}\,,$$
$$\omega_* = \frac{2l\Omega_i}{r_0^2/\rho_s^2}\,,$$

with the validity condition $r_0^2/\rho_s^2 - 4a_{ln} \gg 2l$. The latter is satisfied better for higher n, lower l, smaller R_0, larger r_0 and smaller ρ_s (smaller T_e and larger B). The frequency depends strongly on the plasma size R_0 and the density-gradient scale r_0, besides the effective Larmor radius ρ_s, and the mode numbers l and n. The same is true for the growth–damping rate, which depends also on the collisional plasma parameters $\Gamma_\parallel$ and ν_i, on the current velocity U, and on $k_\parallel$.

The dependence on l and n is not simple. Mode excitation for $n = 1$ was reported in Kauschke et al. (1990). The frequency and the instability rate decrease when n grows, while the collisional damping increases with n. Therefore $n = 0$ modes are usually observed.

When l grows, the frequency can grow, reach a maximum and then decrease, in agreement with numerical results (Kauschke et al. 1990). However, such behaviour depends on R_0 and r_0.

In the approximation of moderate plasma size, when $R_0^2/r_0^2 < x_{ln}$, the Bessel-function zero, the frequency can be also calculated according to (42). In dimensional variables, $K^2 \approx \rho_s^2 x_{ln}^2/R_0^2 \ll 1$,

$$\omega_r = 2l\Omega_i\,\frac{\rho_s^2/r_0^2}{1 + x_{ln}^2\rho_s^2/R_0^2}\,.$$

The eigenfrequency dependence on the magnetic field is similar to that one in the local case. The dependence on the plasma size is important. These are the experimental conditions reported in Ellis and Marden-Marshall (1979) and Ellis et al. (1980), with $R_0^2/r_0^2 = 1.76$, and R_0^2/r_0^2 in the range 0–5 in the numerical analysis.

One might be interested in situations with weak dependence on the plasma radius R_0, which can simulate other plasmas. Such situations correspond to the large-radius approximation, when $R_0^2/r_0^2 \gg 1$. Then the frequency can be calculated according to (48). In dimensional units,

$$\omega_r = \frac{l\Omega_i}{l + 2n + r_0^2/2\rho_s^2}\,,$$

with the validity condition

$$r_0^2 + 4n \gg 2l\rho_s^2.$$

This condition is satisfied better for larger n, larger Gaussian profile widths and plasma radii, for smaller ρ_s (larger magnetic fields and smaller electron tempera-

https://doi.org/10.1017/S002237789900803X Published online by Cambridge University Press

Table 4. Global-theory parameters for the $l = 2$ mode, $\omega_{\rm exper}/\Omega_i = 0.37$; ω_{De} is the 'local theory' parameter; $T_e = 0.5\,$eV corresponds to the probe location; ω is evaluated in the large-radius approximation.

T_e (eV)	r_0^2/ρ_s^2	R_0^2/r_0^2	ω_*/Ω_i	ω/Ω_i	ω_{De}/Ω_i
1.5	4		1	0.5	0.3
1	6	7–12	0.6	0.4	0.2
0.5	12		0.3	0.2	0.1

Table 5. Collisional plasma parameters, $\nu_{en} \approx 500\,$kHz, $\nu_{in} \approx 1\,$kHz, $k_\parallel = k_{\parallel\min}$, $\Gamma_\parallel \approx 2\,$MHz, the dissipative drift-instability threshold for ω_r is $\sqrt{\Gamma_\parallel \nu_{in}} \approx 0.3\Omega_i$, the current convective threshold for ω_r/K^2 is $\Gamma_\parallel \nu_{in}/\omega_U \approx 0.04\Omega_i$ for $\omega_U/\Omega_i = 2$.

λ_{en} (m)	λ_{in} (m)	ν_{en}/Ω_i	ν_{in}/Ω_i	$\Gamma_\parallel/\Omega_i$	$\Gamma_\parallel/\nu_{en}$	$v_{{\rm th},e}k_\parallel/\Omega_i$
1	0.3	3	6×10^{-3}	12	4	5

tures), and for lower azimuthal mode numbers. For the radial mode number $n = 0$, $K^2 \approx 2l/r_0^2 = \omega_*$, with $S \equiv R_0^2 K^2 \approx 2lR_0^2/r_0^2$ being in agreement with the numerical results (Ellis et al. 1980).

An evaluation of the global theory parameters for the experimental conditions in Latten et al. (1995) is presented in Table 4.

In Table 4, ω is evaluated in the large-radius approximation, when the frequency is approximately independent of the macroscopic plasma size. Such a regime might be preferable in the study of the basic drift-wave physics. Otherwise modes dependent on the plasma column radius occur, while this radius cannot be well defined.

The large-radius condition for ρ_s, $r_0^2 + 4n \gg 2l\rho_s^2$, is not met with $T_e = 1.5\,$eV, if one assumes $n = 0$. The magnetic field should be raised at least by a factor of 2–3, or the electron temperature should be decreased by a factor of 5–10, for the same r_0. With a mean temperature of about 1 eV, one finds more favourable estimates. In the same case, the local-theory estimate ω_{De}/Ω_i becomes less favourable. When the temperature is not constant, one can try to develop the theory, taking account of the radial temperature profile.

A nearly vanishing electric field was reported in Latten et al. (1995) (negligible equilibrium $\mathbf{E} \times \mathbf{B}$ rotation), which means that there is no plasma rotation.

Collisional plasma parameters. In Klinger et al. (1997), the mean free paths λ_{en} and λ_{in} for the electron–neutral and ion–neutral collisions are reported. They are given in Table 5, together with other important parameters of collisional (weakly ionized) plasma.

The factor $\nu_i\Gamma_\parallel = k_z^2\mu_e/\mu_i$ includes $\mu = |q|/m\nu$, the mobility of particles of charge q and mass m, as well as the frequency k_z of the ion acoustic waves neglected in the particular case under consideration, $\omega^2 \gg k_z^2$. In the stability domain,

$$|\omega_r| \gg |k_z| \geqslant |\omega_r|\sqrt{\mu_i/\mu_e}\,. \tag{77}$$

This condition requires that

$$\sqrt{\mu_i/\mu_e} \ll 1. \tag{78}$$

Frequently $\mu_i/\mu_e \approx 0.01$. The mobility ratio $\mu_e/\mu_i \gg 1$, which is a function of the gas type only, can be defined from drift measurements. One can evaluate

https://doi.org/10.1017/S002237789900803X Published online by Cambridge University Press

Table 6. Helium and argon plasma characteristics compared, for fixed r_0 and R_0, in the large radius approximation for ω, and when for the argon plasma $\omega_*/\Omega_i < 1$. The table gives the ratios of helium to argon parameters.

m_e/m_i (Ω_i)	α_i	v_s, v_A, $v_{\mathrm{th},\,i}$	ρ_s (r_0^2/ρ_s^2)
10	0.1	$\sqrt{10}$	$1/\sqrt{10}$ (10)
ω_*/Ω_i	ω_*	ω/Ω_i	ω
0.1	1	~ 0.1	~ 1

(Delcroix 1966)

$$\frac{\mu_i}{\mu_e} \sim \frac{\sigma_{en}}{\sigma_{in}} \sqrt{\frac{m_e}{m_i}\frac{T_e}{T_i}}, \tag{79}$$

where σ_{en} (σ_{in}) is the cross-section for electron–neutral (ion-neutral) collisions.

Thus, according to (77), the threshold for the weak drift-dissipative instability can be also evaluated as

$$\omega_r > \frac{|k_z|}{\sqrt{\mu_i/\mu_e}}. \tag{80}$$

The terms $\nu\mathbf{v}$ in (2) can take account of other dissipation mechanisms due to collisions, besides the collisions with neutrals in partially ionized plasmas, for example the electron–ion collisions in fully ionized plasmas when the motion parallel to **B** is studied. In the latter case, $\nu\mathbf{v}_\perp$ is replaced with $-\mu\Delta\mathbf{v}_\perp$, which takes account of finite plasma viscosity μ (Braginskii 1965; Okuda and Dawson 1973).

The fluid description of electrons is valid when

$$\Gamma_\parallel \ll \nu_{en}\,. \tag{81}$$

The adiabatic regime for the electrons implies another constraint on $\Gamma_\parallel$:

$$\omega_U,\ \omega \ll \Gamma_\parallel = D_e k_\parallel^2\,. \tag{82}$$

When

$$\Gamma_\parallel \gtrsim \nu_{en}\,, \tag{83}$$

the kinetic description of electrons is relevant. In the limit

$$\omega,\ \nu_{en} < |v_{\mathrm{th},\,e}k_\parallel| \to \Gamma_\parallel \gg \nu_{en}\,, \tag{84}$$

the electrons can be treated as collisionless, with the adiabatic density response $\delta n_e/n_{e0} = \delta\phi/\tau$ in the first approximation, similar to the regime (81). In this limit, the plasma oscillations are governed by (31), with K^2 from (32).

7.3. Comparison of helium and argon plasmas

Table 6 compares the parameters and global-theory predictions for helium and argon plasmas, for fixed r_0 and R_0, in the large-radius approximation for ω, and when, for the argon plasma, $\omega_*/\Omega_i < 1$.

For the same k_z, the coupling to ion acoustic waves becomes stronger in the helium plasma. The theoretical predictions of the low-frequency oscillations in the helium plasma are more favourable. Electromagnetic effects are weaker in the helium plasma and are less favourable for observations. The ratio for the drift-instability threshold $\sqrt{\nu_{in}\Gamma_\parallel}$ is evaluated to be of the order of $10^{1/4}$ for the same cross-sections of charge–neutral collisions.

https://doi.org/10.1017/S002237789900803X Published online by Cambridge University Press

8. Conclusions

The linear and nonlinear properties of collective oscillations in a cylindrical magnetized laboratory plasma have been investigated analytically within the context of the self-consistent field description based on the Tonks–Langmuir fluid model for the weakly ionized (collisional) plasma.

In the linear theory, the system is treated as an eigenvalue problem. The various *destabilization mechanisms* have been carefully revisited and identified for the interesting collisional plasma model. These are drift-dissipative instability, and the current convective or spiral instability. Our analytical results are in accordance with local theory and numerical results obtained previously. Several errors in the existing literature have been pointed out.

This investigation allows for a detailed *comparison between the theoretical models and experimental results* with regard to possible *scenarios of instability and transition to turbulence*, and with regard to the dependences of *eigenfrequencies* and *instability rates* on plasma parameters. Such a comparison can be used as a basis for developing effective methods for *turbulence control* by *taming the instability in the coherent plasma state* already. Several important plasma parameters that can be controlled in experiments are included in the theory. These are the *density and temperature profiles, equilibrium flows, effective collision frequencies with neutrals and ionization rates*, and *axial magnetic field strength*.

Comparison with experimental results shows that the basic local and global dispersion relations for the low-frequency drift waves are not generally valid in the reported measurements. In particular, for a control parameter leading to a turbulent spectrum, the unstable modes occur at frequencies in the range of the ion cyclotron frequency and its harmonics. As a consequence, it is not clear whether or not this situation can be labelled *drift-wave turbulence*.

The analysis of important parameters of collisions shows that experiments with cylindrical plasmas are frequently carried out under the conditions beyond the domain of validity of the fluid description of electrons, and non-collisional physics of collective oscillations can become important. Then one should also be careful before labelling a particular plasma state *collisional* drift-wave turbulence.

In the simplest case, the Vlasov drift-kinetic description of electrons is required. In a more complicated general case, the experimental conditions can correspond to the transition between the fluid and kinetic regimes for electrons, when kinetic effects cannot be disregarded. Then the collision integral must be included in the drift-kinetic theory. For electron–neutral collisions in a weakly ionized plasma (or electron–ion collisions in a fully ionized plasma), one can use simplified Bhatnagar–Gross–Krook types of collision integral. The latter are also used frequently to model turbulent plasma states.

Transition from collisional to non-collisional physics is an important problem for fusion plasmas. Another is *transition from a regular to a turbulent plasma state*. Electrostatic drift-wave turbulence and related anomalous plasma transport in the tokamak edge region, where collisions are of crucial importance, attract particular attention. Thus experiments with small laboratory devices containing weakly ionized plasmas and theories of collective oscillations in these plasmas can have special relevance for controlled fusion studies. Such experiments and theories allow us to test our understanding of basic plasma physics, including particle collisions and turbulence, to elucidate possible mechanisms of anomalous transport, and to develop

https://doi.org/10.1017/S002237789900803X Published online by Cambridge University Press

new and reliable methods of *plasma diagnostics and control* (Sosenko and Grésillon 1993, 1994; Sosenko et al. 1995, 1996, 1997; Klinger et al. 1997a; Bonhomme et al. 1998; Doviel and Equipe Turbulence Plasma 1998; Grésillon and Tomchuk 1998a,b; Sosenko and Pierre (1998).

Frequently, the cylindrical plasma situations are specified as *low-β* or *very low-β* (Klinger et al. 1997a; Bonhomme et al. 1998). Our estimates show that the parameter β in argon can be very small but still comparable with the *electron–ion mass ratio*. Then the *electrostatic approximation* is not applicable in the general case, and *magnetic field fluctuations* can come into play. Preliminary theoretical and experimental results (Sosenko and Pierre 1998) confirm this interesting point and suggest new diagnostics for the magnetic field fluctuations. The controversial understanding of the role of such fluctuations in fusion plasmas can be mentioned in this regard. Possibilities for illuminating the role of magnetic fluctuations and developing their diagnostics by studies of both cylindrical and toroidal plasmas in small laboratory devices must be considered.

Generalizations to situations with plasma rotation, for arbitrary frequencies and for hybrid fluid–kinetic regimes with collisional and non-collisional physics will be considered in subsequent papers, as will situations with magnetic fluctuations.

The cold-fluid approximation is used here for ions. This is usually sufficient for the description of weakly ionized plasmas with $T_e \gg T_i$. One can see that for the parameters from Tables 2 and 3, $v_{\mathrm{th},i}k_\parallel/\Omega_i \approx 0.004 \ll \omega/\Omega_i$, and the ion Larmor radius ρ_{Li} is very small, $\rho_{Li}^2 k_\perp^2 \approx 0.01$; therefore the cold-ion approximation is justified for both parallel and perpendicular particle motions. In order to investigate the fine effects of thermal ion motion, a kinetic (gyrokinetic) description can be required. This is beyond the scope of the present study.

Owing to the cylindrical magnetic field configuration in the experiments considered, the magnetic field curvature is very weak in the part of the devices where the drift waves are excited, which usually precludes the investigation of the curvature effect on drift waves – on ion drift modes in particular. Our purpose here is to investigate the stability of the linear plasma column. Of course, the situation would be more relevant for the comparison with tokamak plasmas if the magnetic field curvature were introduced. The various instability mechanisms can lead to a very complicated situation, and an experimental study of the evolution of the plasma column stability starting from the linear column and progressively changing the curvature would certainly be fruitful.

Our comparison of theory and experimental observations shows that many physical parameters can be important; therefore one must be careful in any close comparison of experimental data with theoretical predictions. Frequently, a numerical study of nonlinear models is required to explain the observations of turbulent or chaotic plasma states.

Though we have also given some general nonlinear models, the main purpose of this paper was to study the linear properties of global modes, and to give a detailed classification of possible physical regimes. The quantitative analysis of nonlinear properties, for example saturation levels, together with numerical modelling will be the next stage of our study, and will be presented elsewhere. Our nonlinear models are similar to other reduced fluid plasma models. Thus we believe that they contain all the necessary ingredients that can lead to various nonlinear coupling regimes like self-sustained turbulence with many modes excited, or spatio-temporal chaos

https://doi.org/10.1017/S002237789900803X Published online by Cambridge University Press

when only few modes are excited. Experimental observations make this suggestion credible.

Acknowledgements

Discussions with Drs Gérard Leclert, Dominique Grésillon, Fabrice Doveil, Thomas Klinger, Yves Elskens, Pierre Bertrand and Giovanni Manfredi are very much appreciated.

Appendix A. Confluent hypergeometric function

The confluent hypergeometric function $M(a, b, z)$ of z is governed by the differential equation

$$zM'' + (b - z)M' - aM = 0\,.$$

The solution can be found as a series

$$M(a, b, z) = 1 + \frac{a}{b}\,\frac{z}{1!} + \frac{a(a+1)}{b(b+1)}\,\frac{z^2}{2!} + \frac{a(a+1)(a+2)}{b(b+1)(b+2)}\,\frac{z^3}{3!} + \dots\,,$$

convergent for finite z, with $b \neq 0, -1, -2, -3, \dots$.

$a_{ln}(z)$ denotes a real root of the equation $M(a, l+1, z) = 0$, $n = 0, 1, \dots$. Evidently $a_{ln} < 0$. For example, when $z = l + 1$, $a = -1$ is one root. Or when $z = l + 2 \pm \sqrt{l+2}$, $a = -2$ is a root.

$a_{ln}(z)$ can easily be found by using *Maple V Release 4*. (The case $l = 0$, which is not interesting, is presented in Abramowitz and Stegun (1964) for $1 \leqslant z \leqslant 3.39$, with $-1 \leqslant a \leqslant -0.1$.)

In general, $|a|$ decreases when z grows, but grows when l grows.

When $z \gg 1$, $|a_{ln} + n| \ll 1$ for not very large l. Thus the approximate roots are

$$a_{ln} \sim -n, \qquad z \gg 1\,.$$

For example,

$$a_{l0} \sim -\frac{l+1}{z} \Big/ \left[1 + \frac{z}{2(l+2)} + \frac{z^2}{3(l+2)(l+3)} + \dots\right],$$

$$a_{l1} \sim -1 - \left(1 - \frac{l+1}{z}\right) \Big/ \left[1 + \frac{z}{2!(l+2)} + \frac{z^2}{3!(l+2)(l+3)} + \frac{2!z^3}{4!(l+2)(l+3)(l+4)} + \dots\right].$$

The numerical values of zeros are given in Table A.1.

Table A.1. Zeros $a_{ln}(z)$ of the hypergeometric function, $M(a, l+1, z) = 0$, for $z = 16$.

	$n = 0$	$n = 1$	$n = 2$	$n = 3$
$l = 1$	−0.000 024 891 914 35	−1.001 978 447	−2.034 591 935	−3.209 236 900
$l = 2$	−0.000 183 050 071 4	−1.008 026 783	−2.086 420 159	−3.374 309 614
$l = 3$	−0.000 889 215 555 7	−1.023 998 380	−2.175 008 069	−3.592 202 262
$l = 4$	−0.003 210 254 341	−1.057 090 704	−2.305 287 207	−3.860 445 343
$l = 5$	−0.009 212 164 260	−1.114 275 984	−2.478 663 419	−4.176 415 870
$l = 6$	−0.022 017 765 65	−1.200 808 472	−2.694 696 583	−4.537 913 151
$l = 7$	−0.045 460 660 85	−1.319 868 134	−2.952 327 886	−4.943 227 378
$l = 8$	−0.083 532 019 82	−1.473 020 505	−3.250 468 570	−5.391 059 395

https://doi.org/10.1017/S002237789900803X Published online by Cambridge University Press

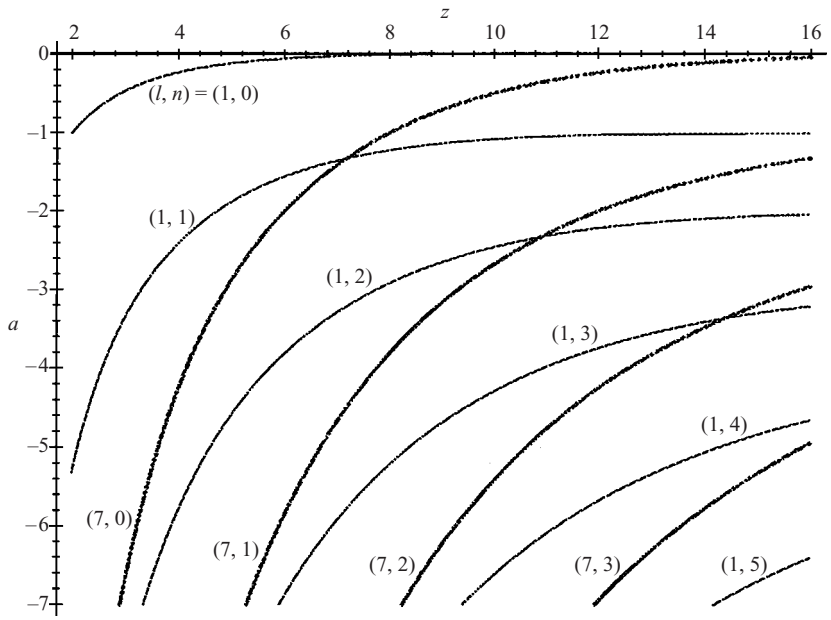


Figure A.1. Zeros $a_{ln}(z)$ of the hypergeometric function, $M(a, l + 1, z) = 0$, for $l = 1$ and 7.

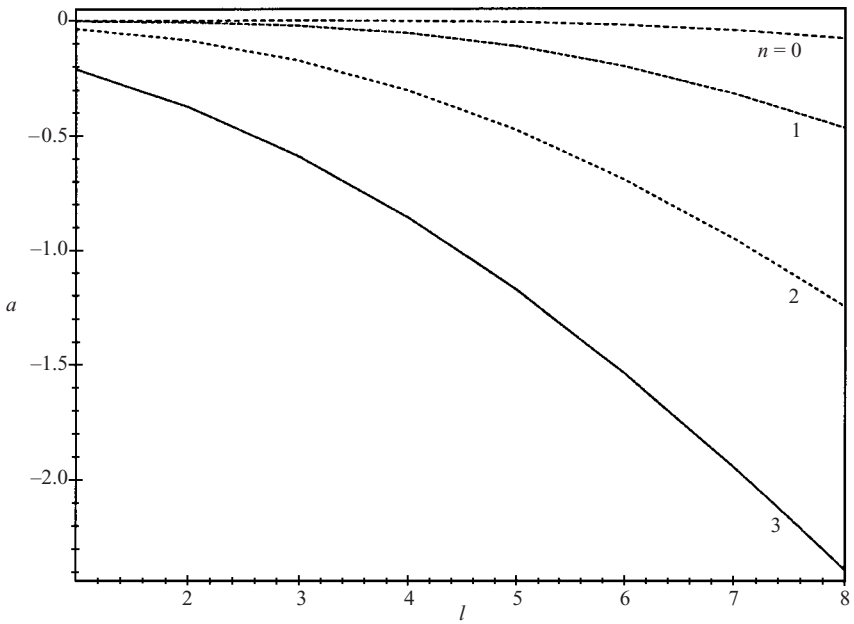


Figure A.2. Zeros $a_{ln}(z)$ of the hypergeometric function, $M(a, l + 1, z) = 0$, for $l = 1, \ldots, 8$, $n = 0, \ldots, 3$ and $z = 16$

https://doi.org/10.1017/S002237789900803X Published online by Cambridge University Press

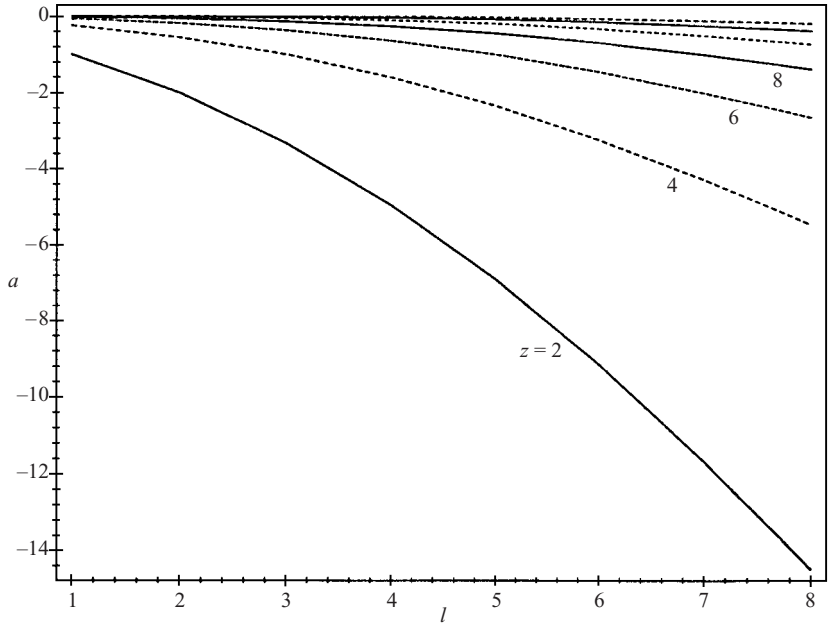


Figure A.3. Zeros $a_{ln}(z)$ of the hypergeometric function, $M(a, l+1, z) = 0$, for $l = 1, \ldots, 8$, $n = 0$ and $z = 2, \ldots, 14$.

Figures A.1–A.3 show the dependence of a_{ln} on l, n and z.

Appendix B. Eigenfunctions and eigenfrequencies

Figures B.1–B.4 show the radial dependence of the exact eigenfunctions

$$\sim r^l M(a_{ln}(z_0),\ l+1,\ r^2 z_0)$$

in the case of a Gaussian density profile for $l = 1, \ldots 8$, $n = 0, \ldots 3$, $z_0 \equiv (R_0/r_0)^2 = 2, \ldots, 16$. r is normalized to R_0 the plasma radius. The modes with higher l and n and larger z_0 are more localized towards the plasma edge, $r \gtrsim 0.8$ (except for $z_0 = 2$). At the same time, the density gradient is largest at $r^2 = (2z_0)^{-1}$; that is, the density gradient is maximum in the domain $r \leqslant 0.5$ (e.g. $r = 0.25$ for $z_0 = 8$).

Figure B.5 shows the dependence of the eigenvalues $r_0^2 K_{ln}^2 = 2l - 4a_{ln}$ on l, when $n = 0$, for various values of $z_0 \equiv (R_0/r_0)^2$. When z_0 increases, K_{ln}^2 decreases; and when z_0 increases, one observes a transition from the nonlinear dependence on l to an approximately linear dependence $K_{ln}^2 \approx 2l$.

Figure B.6 shows the eigenfrequency dependence on l and R_0, for $n = 0$, in the case of a Gaussian density profile, in the weakly non-adiabatic regime. As a function of l, the frequency can have a maximum for small enough values of $z_0 \equiv (R_0/r_0)^2$, or it can grow monotonically with l and saturate for large enough z_0. When $z_0 = 2$, the frequency has a broad maximum at $l = 3$. When R_0 grows, the maximum shifts to larger l and becomes broader; then it disappears, and the frequency grows and saturates with R_0.

Figures B.7 and B.8 show the dependence on l and $z_0 \equiv (R_0/r_0)^2$ of the part

https://doi.org/10.1017/S002237789900803X Published online by Cambridge University Press

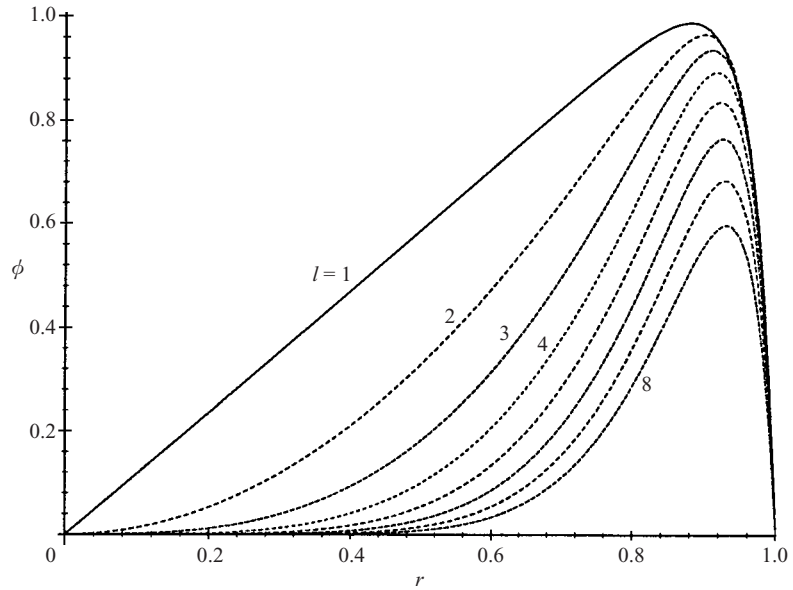


Figure B.1. Radial dependence of exact eigenfunctions $\sim r^l M(a_{ln}(z_0),\ l+1,\ r^2 z_0)$ for $l = 1, \ldots, 8$, $n = 0$ and $z_0 \equiv R_0^2/r_0^2 = 16$.

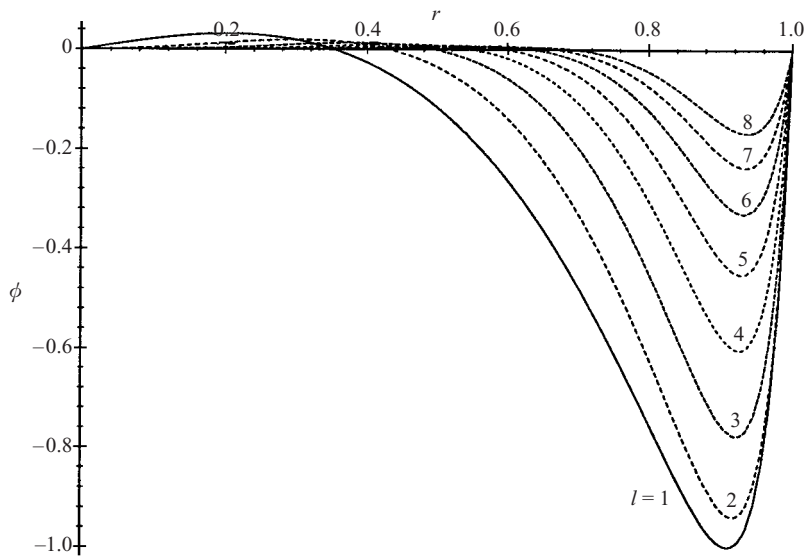


Figure B.2. Radial dependence of exact eigenfunctions $\sim r^l M(a_{ln}(z_0),\ l+1,\ r^2 z_0)$ for $l = 1, \ldots, 8$, $n = 1$ and $z_0 \equiv R_0^2/r_0^2 = 16$.

$\gamma_{\rm dis} = \omega_r^2 K^2/\Gamma_\parallel(1+K^2) \sim l^2 K^2/(1+K^2)^3$ of the instability rate due to the dissipative mechanism alone, for $n = 0$, in the case of a Gaussian density profile, in the weakly non-adiabatic regime. $\gamma_{\rm dis}$ has a behaviour similar to that of the frequency. When $z_0 = 2$, $\gamma_{\rm dis}$ has a broad maximum at $l = 3$. This maximum is more pronounced when $z_0 = 4$. It shifts to $l = 4$ when $z_0 = 6$, and to $l = 5$ when $z_0 = 8$, and so on.

https://doi.org/10.1017/S002237789900803X Published online by Cambridge University Press

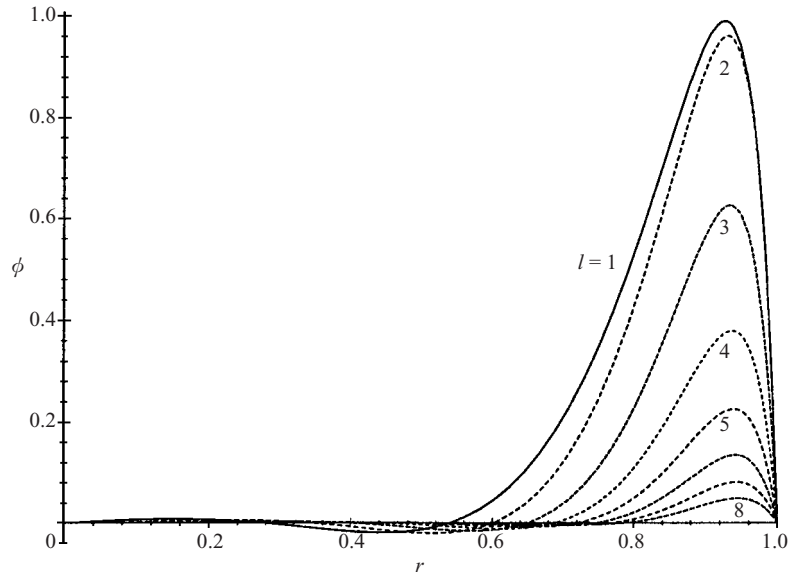


Figure B.3. Radial dependence of exact eigenfunctions $\sim r^l M(a_{ln}(z_0),\ l+1,\ r^2 z_0)$ for $l = 1, \ldots, 8$, $n = 2$ and $z_0 \equiv R_0^2/r_0^2 = 16$.

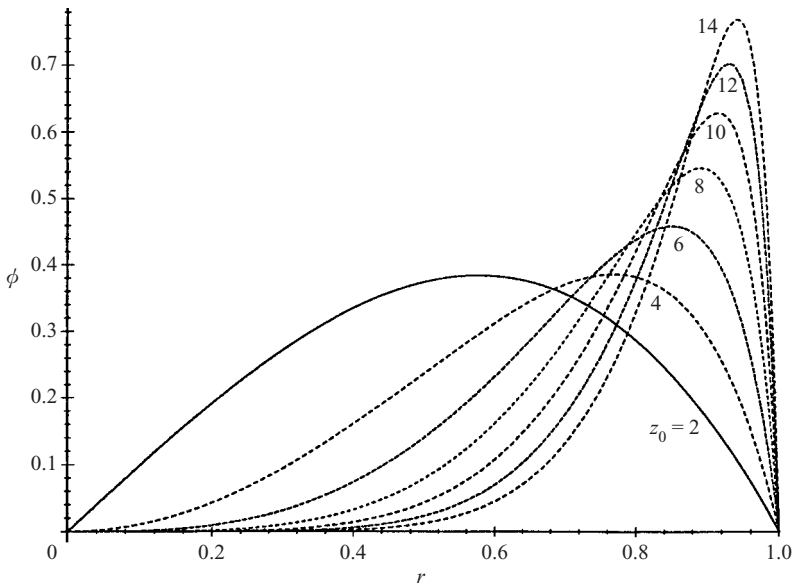


Figure B.4. Radial dependence of exact eigenfunctions $\sim r^l M(a_{ln}(z_0),\ l+1,\ r^2 z_0)$ for $l = 1$, $n = 0$ and $z_0 = 2, \ldots, 14$.

For sufficiently large R_0, $\gamma_{\rm dis}$ grows and saturates when l grows. When R_0 grows, $\gamma_{\rm dis}$ grows and saturates for fixed l.

Figure B.9 shows the dependence on l and $z_0 = (R_0/r_0)^2$ of the part $\gamma_{\rm cur} = \omega_U \omega_r / \Gamma_\parallel (1+K^2) \sim l/(1+K^2)^2$ of the instability rate due to the current mechanism alone on l and $z_0 \equiv (R_0/r_0)^2$ for $n = 0$, in the case of a Gaussian density profile,

https://doi.org/10.1017/S002237789900803X Published online by Cambridge University Press

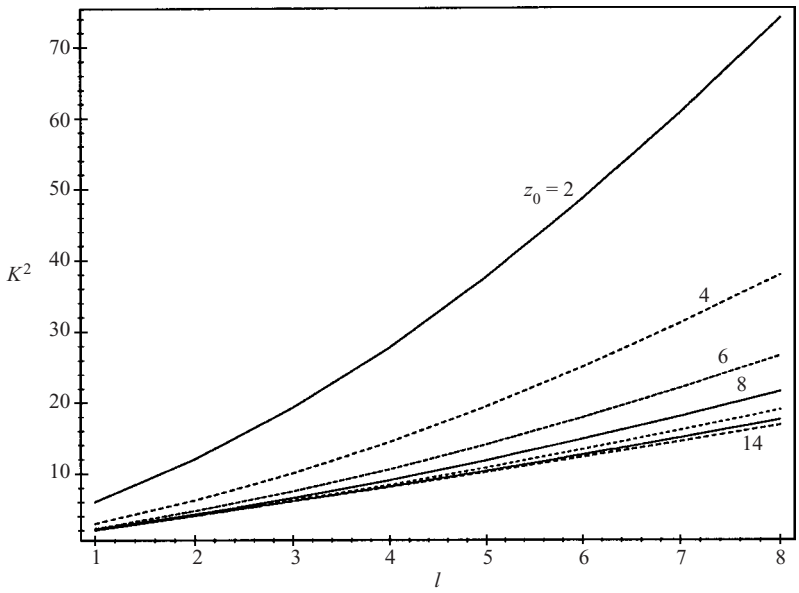


Figure B.5. Eigenvalues $r_0^2 K_{ln}^2 = 2l - 4a_{ln}$ for $l = 1, \ldots, 8$, $n = 0$ and $z_0 = 2, \ldots, 14$.

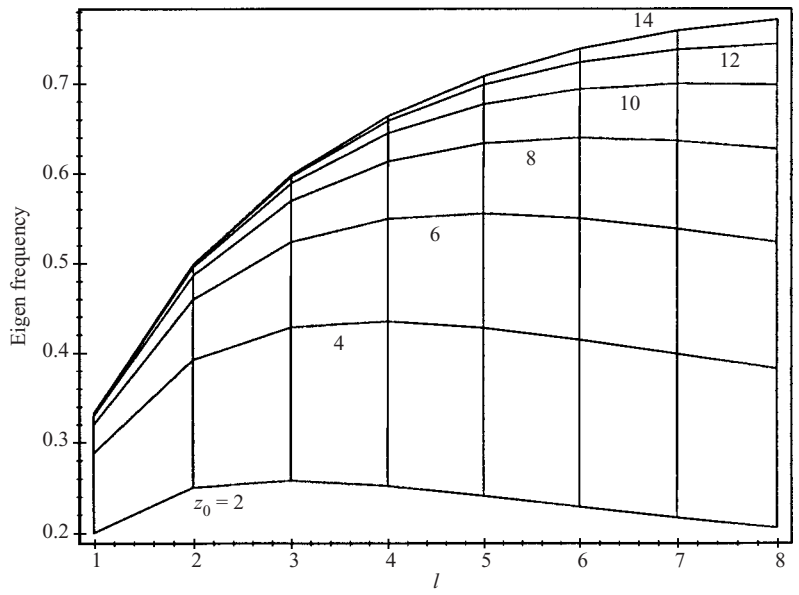


Figure B.6. Eigenfrequencies in the weakly non-adiabatic regime for $l = 1, \ldots, 8$, $z_0 = 2, \ldots, 14$ and $n = 0$.

in the weakly non-adiabatic regime. For a fixed z_0, $\gamma_{\rm cur}$ also has a maximum as a function of l, which is narrower than that of $\gamma_{\rm dis}$ and which is attained at different values of l. When $z_0 = 2$ or 4, $\gamma_{\rm cur}$ has a maximum at $l = 1$. This maximum shifts to $l = 2$ when $z_0 = 6, \ldots, 14$. When $z_0 = 6$, the mode $l = 1$ dominates over the mode $l = 3$, but when z_0 is large enough, the mode $l = 3$ dominates over the mode $l = 1$.

https://doi.org/10.1017/S002237789900803X Published online by Cambridge University Press

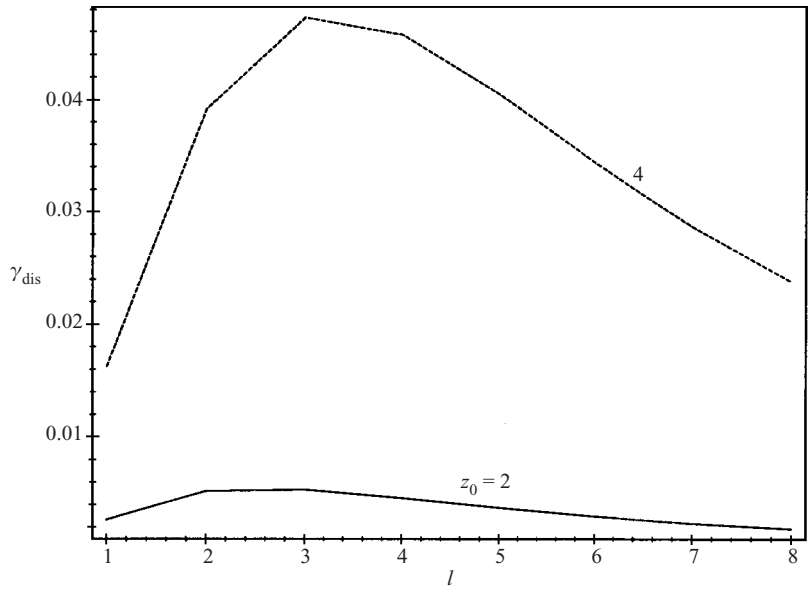


Figure B.7. Instability rate $\gamma_{dis} = \omega_r^2 K^2/\Gamma_\parallel(1+K^2) \sim l^2K^2/(1+K^2)^3$ due to the dissipative mechanism alone in the weakly non-adiabatic regime for $l = 1 \ldots, 8$, $z_0 = 2$ and 4, and $n = 0$.

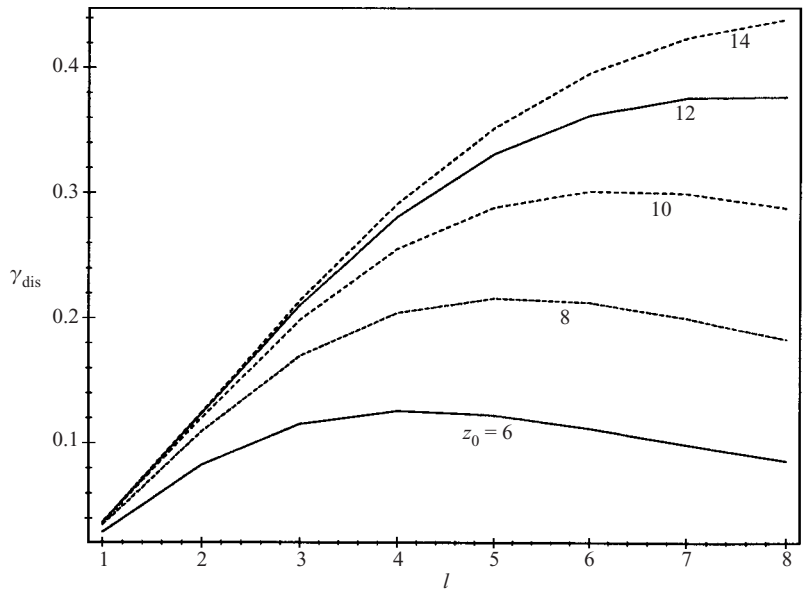


Figure B.8. Instability rate $\gamma_{\rm dis} = \omega_r^2 K^2/\Gamma_\parallel(1+K^2) \sim l^2K^2/(1+K^2)^3$ due to the dissipative mechanism alone in the weakly non-adiabatic regime for $l = 1, \ldots, 8$, $z_0 = 6, \ldots, 14$ and $n = 0$.

https://doi.org/10.1017/S002237789900803X Published online by Cambridge University Press

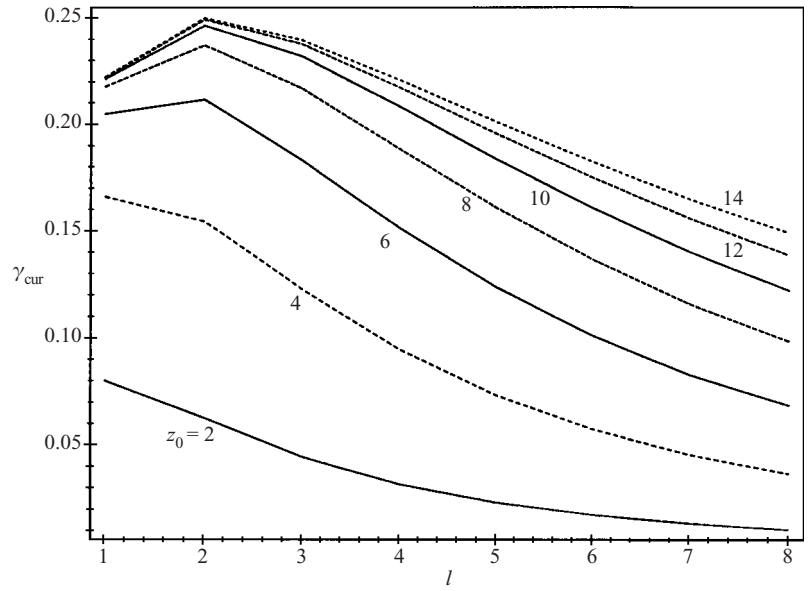


Figure B.9. Instability rate $\gamma_{\rm cur} = \omega_U \omega_r / \Gamma_\parallel (1 + K^2) \sim l/(1 + K^2)^2$ due to the current mechanism alone in the weakly non-adiabatic regime for $l = 1, \ldots, 8$, $z_0 = 2, \ldots, 14$ and $n = 0$.

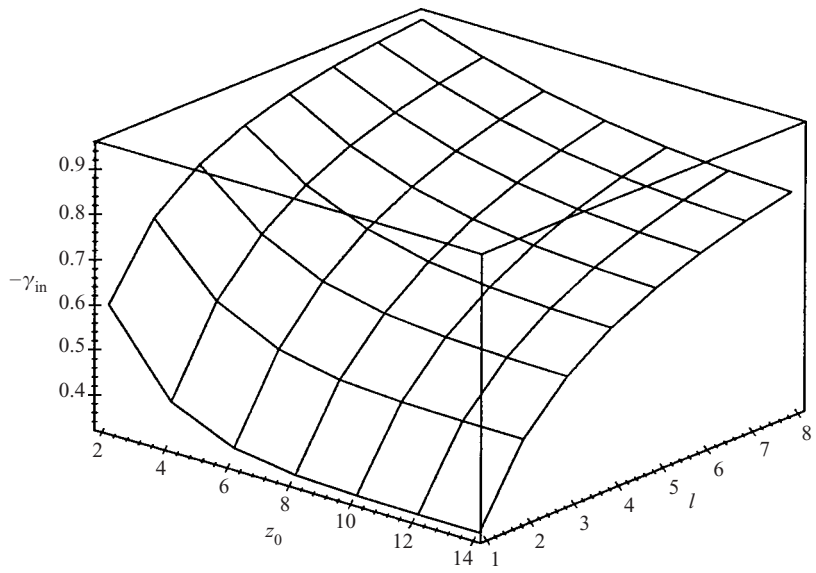


Figure B.10. Dissipation rate $-\gamma_{in} = \nu_i K^2/(1 + K^2) \sim K^2/(1 + K^2)$ due to ion–neutral collisions in the weakly non-adiabatic regime for $l = 1, \ldots, 8$, $z_0 = 2, \ldots, 14$ and $n = 0$.

For sufficiently large R_0, $\gamma_{\rm dis}$ grows, and saturates when l grows. When R_0 grows, $\gamma_{\rm cur}$ also grows and saturates for fixed l.

Figure B.10 shows the dependence on l and $z_0 \equiv (R_0/r_0)^2$, of the part $-\gamma_{in} = \nu_i K^2/(1 + K^2) \sim K^2/(1 + K^2)$ of the damping rate due to ion–neutral collisions, for

https://doi.org/10.1017/S002237789900803X Published online by Cambridge University Press

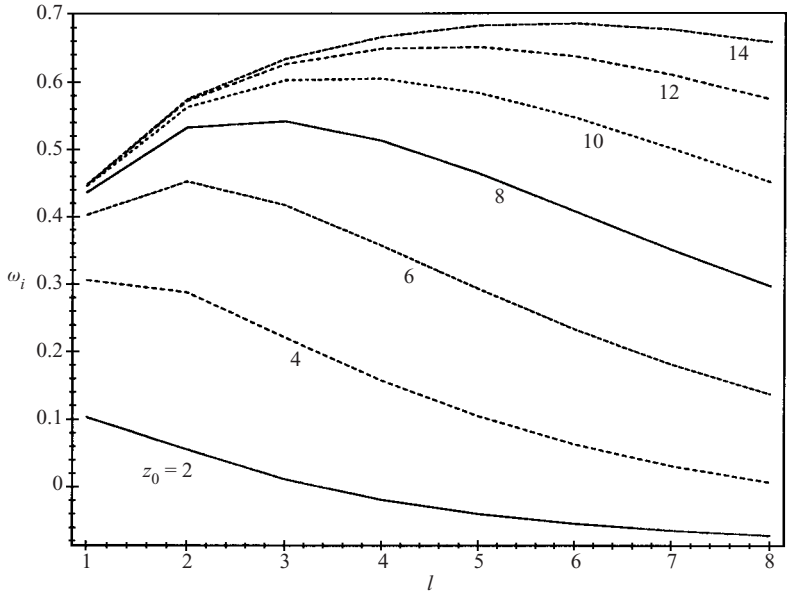


Figure B.11. Total growth–damping rate $\omega_i = K^2(\omega_r^2/\Gamma_\parallel + \omega_U\omega_r/\Gamma_\parallel K^2 - \nu_i)/(1+K^2)$ in the weakly non-adiabatic regime for $l = 1, \ldots, 8$, $z_0 = 2, \ldots, 14$, $n = 0$, $\nu_i\Gamma_\parallel = 0.1$, $\omega_U = 2$ and $r_0^2 = 2$.

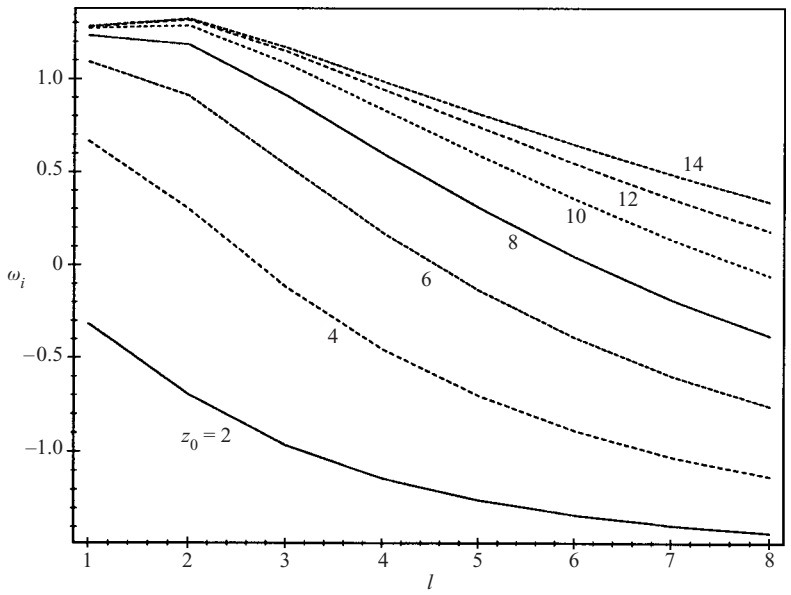


Figure B.12. Total growth–damping rate $\omega_i = K^2(\omega_r^2/\Gamma_\parallel + \omega_U\omega_r/\Gamma_\parallel K^2 - \nu_i)/(1+K^2)$ in the weakly non-adiabatic regime for $l = 1, \ldots, 8$, $z_0 = 2, \ldots, 14$, $n = 0$, $\nu_i\Gamma_\parallel = 0.1$, $\omega_U = 2$ and $r_0^2 = 4$.

https://doi.org/10.1017/S002237789900803X Published online by Cambridge University Press

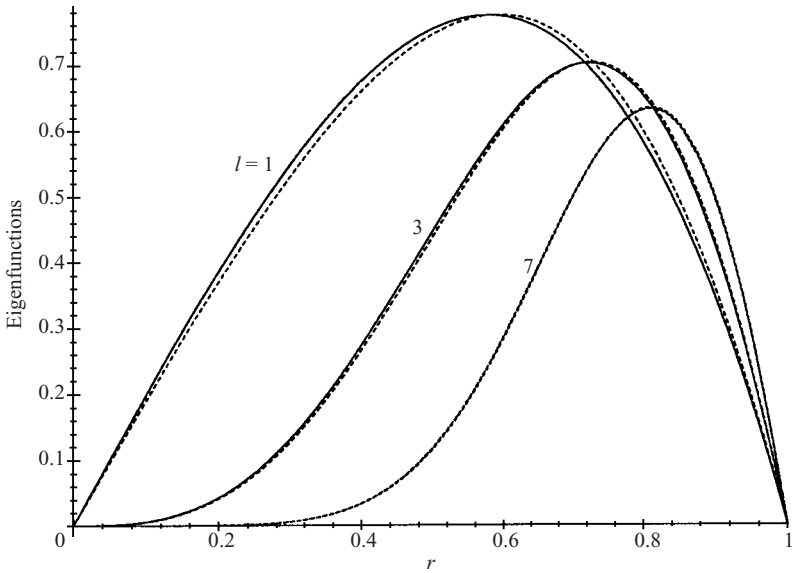


Figure B.13. Comparison of exact eigenfunctions (solid lines) and eigenfunctions (dashed lines) in the moderate-radius approximation for $l = 1$, 3 and 7, $z_0 = 2$ and $n = 0$.

$n = 0$, in the case of a Gaussian density profile, in the weakly non-adiabatic regime. $-\gamma_{in}$ grows when l or $1/R_0$ grows.

Figures B.11 and B.12 show the dependence of the total growth–damping rate

$$\omega_i = \left(\frac{\omega_r^2}{\Gamma_\parallel} + \frac{\omega_U \omega_r}{\Gamma_\parallel K^2} - \nu_i\right) \frac{K^2}{1+K^2}$$
$$\sim \frac{l^2 K^2}{(1+K^2)^3} + \frac{\omega_U r_0^2}{2} \frac{l}{(1+K^2)^2} - \frac{\nu_i \Gamma_\parallel r_0^4}{4} \frac{K^2}{1+K^2}$$

on l and R_0, for $n = 0$, in the case of a Gaussian density profile, in the weakly non-adiabatic regime, with $\omega_U = 2$, $\nu_i \Gamma_\parallel = 0.1$, $r_0^2 = 2,\ 4$. When l or R_0 grows, there are transitions from one dominant-mode regime to another according to the properties of $\gamma_{\rm dis}$, $\gamma_{\rm cur}$ and $\gamma_{\rm in}$, and with their relative contributions determined by the dimensionless parameters ω_U, $\nu_i \Gamma_\parallel$ and r_0^2 (or ω_U/Ω_i, $\nu_i \Gamma_\parallel / \Omega_i^2$, r_0^2/ρ_s^2 in dimensional units). For sufficiently large R_0, $\gamma_{\rm dis}$ dominates, and a rather broad mode spectrum can be excited.

Figure B.13 presents a comparison of the exact eigenfunctions

$$\sim r^l M(a_{ln},\ l+1,\ r^2 z_0)$$

and the eigenfunctions in the moderate-radius approximation

$$\sim \exp\left(\tfrac{1}{2} r^2 z_0\right)\ J_l(x_{ln} r)$$

for $l = 1$, 3 and 7, $z_0 = 2$ and $n = 0$.

References

Abramowitz, M. and Stegun, I. A. 1964 *Handbook of Mathematical Functions*. Dover, New York.

Bachet, G., Chérigier, L., Carrere, M. and Doveil, F. 1993 *Phys. Fluids* **B5**, 3097–3102.

https://doi.org/10.1017/S002237789900803X Published online by Cambridge University Press

Bonhomme, G., Pierre, Th., Leclert, G. and Trulsen, J. 1991 *Plasma Phys. Contr. Fusion* **33**, 507–520.

Bonhomme, G., Pierre, Th., Caron, X. and Gravier, E. 1998 In: *Exposés des Journées CEA/CNRS/Universités Sur la Fusion Magnétique, Cadarache, 23 et 24 Novembre 1998*.

Braginskii, S. I. 1965 In: *Reviews of Plasma Physics*, Vol. 1 (ed. M. A. Leontovich), pp. 205–311. Consultants Bureau, New York.

Delcroix, J. L. 1966 *Physique des Plasmas*. Tome 2. *Gaz faiblement ionisés*. Dunod, Paris.

Doveil, F. and Equipe Turbulence Plasma 1998 In: *Exposés des Journées CEA/CNRS/ Universités Sur la Fusion Magnétique, Cadarache, 23 et 24 Novembre 1998*.

Ellis, R. F. and Marden-Marshall, E. 1979 *Phys. Fluids* **22**, 2137–2139.

Ellis, R. F., Marden-Marshall, E. and Majeski, R. 1980 *Plasma Phys.* **22**, 113–132.

Gravier, E. 1999 Etude expérimentale des régimes dynamiques des ondes de dérive dans un plasma magnétisé de laboratoire. Contrôle du chaos spatio-temporel. Thèse de l'Univerité Henri Poincaré, Nancy I.

Gravier, E., Caron, X., Bonhomme, G. and Pierre, Th. 1999 *Phys. Plasmas* **6**, 1670–1673.

Grésillon, D. and Tomchuk, B. 1998a In: *Exposés des Journées CEA/CNRS/Universités Sur la Fusion Magnétique, Cadarache, 23 et 24 Novembre 1998*.

Grésillon, D. and Tomchuk, B. 1998b In: *Exposés des Journées CEA/CNRS/Universités Sur la Fusion Magnétique, Cadarache, 23 et 24 Novembre 1998*.

Grulke, O., Klinger, T. and Piel, A. 1999 *Phys. Plasmas* **6**, 788–796.

Hasegawa, A. and Mima, K. 1978 *Phys. Fluids* **21**, 87–91.

Hasegawa, A. and Wakatani, M. 1983 *Phys. Rev. Lett.* **50**, 682–686.

Hasegawa, A. and Wakatani, M. 1984 *Phys. Fluids* **27**, 611–618.

Kadomtsev, B. B. 1965 *Plasma Turbulence*. Academic Press, New York.

Kauschke, U., Oelerich-Hill, G. and Piel, A. 1990 *Phys. Fluids* **B2**, 38–43.

Klinger, T., Latten, A., Piel, A., Bonhomme, G., Pierre, Th. and Dudok de Wit, T. 1997a *Phys. Rev. Lett.* **79**, 3913–3916.

Klinger, T., Latten, A., Piel, A., Bonhomme, G. and Pierre Th. 1997b *Plasma Phys. Contr. Fusion* **39**, B145–B156.

Latten, A., Klinger, T., Piel, A. and Pierre, Th. 1995 *Rev. Sci. Instrum.* **66**, 3254–3262.

Marden-Marshall, E. and Hall, K. L. 1986 *Plasma Phys. Contr. Fusion* **28**, 1867–1884.

Marden-Marshall, E., Ellis, R. F. and Walsh, J. E. 1986 *Plasma Phys. Contr. Fusion* **28**, 1461–1482.

Okuda, H. and Dawson, J. M. 1973 *Phys. Fluids* **16**, 408–426.

Pierre, Th., Bonhomme, G. and Cussenot, J. R. 1981 *C.R. Acad. Sci. Paris, Sér. II* **293**, 413–416.

Pierre, Th., Bonhomme, G., Cussenot, J. R. and Leclert, G. 1983a *Phys. Lett.* **95A**, 159–161.

Pierre, Th., Bonhomme, G., Cussenot, J. R. and Leclert, G. 1983b *J. Phys. (Paris) Lett.* **44**, L629–634.

Pierre, Th., Bonhomme, G., Leclert, G. and Cussenot J. R. 1985a *Plasma Phys. Contr. Fusion* **27**, 523–526.

Pierre, Th., Bonhomme, G., Leclert, G. and Cussenot, J. R. 1985b *Plasma Phys. Contr. Fusion* **27**, 1497–1508.

Pierre, Th., Rhode, V. and Piel, A. 1992 *Phys. Fluids* **B4**, 2661–2664.

Pierre, Th., Leclert, G. and Braun, F. 1987 *Rev. Sci. Instrum.* **58**, 6–11.

Pisani, F., Pierre, T. and Batani, D. 1998 *J. Plasma Phys.* **59**, 69–82.

Self, S. A. and Ewald H. N. 1966 *Phys. Fluids* **9**, 2486–2492.

Sitenko, A. and Malnev, V. 1995 *Plasma Physics Theory*. Chapman & Hall, London.

Sosenko, P. P. and Grésillon, D. 1993 In: *Proceedings of the 20th EPS Conference on Controlled Fusion and Plasma Physics (26–30 July 1993, Lisboa, Portugal), Contributed Papers* (ed. J. A. Costa Cabral, M. E. Manso, F. M. Serra and F. C. Schuller), Part III. pp. 1239–1249.

Sosenko, P. P. and Grésillon, D. 1994 *Physica Scripta* **50**, 716–719.

Sosenko, P. and Pierre, Th. 1998 In: *Exposés des Journées CEA/CNRS/Universités Sur la Fusion Magnétique, Cadarache, 23 et 24 Novembre 1998*.

Sosenko, P., Maafa, N. and Grésillon, D. 1995 *Physica Scripta* **51**, 647–654.

https://doi.org/10.1017/S002237789900803X Published online by Cambridge University Press

Sosenko, P. P., Grésillon, D. and Maafa, N. 1996 *J. Atmos. Terrest. Phys*. **58**, 1047–1062.

Sosenko, P., Sitenko, A. and Grésillon, D. 1997 *Ukr. J. Phys*. **42**, 38–40.

Tonks, L. and Langmuir, I. 1929 *Phys. Rev*. **33**, 195; also in *The Collected Works of Irving Langmuir*. Vol. 5. *Plasma and Oscillations*, (ed. C. G. Suits and H. E. Way), pp. 122–139. Pergamon Press, Oxford, 1961.

https://doi.org/10.1017/S002237789900803X Published online by Cambridge University Press